A review of Oceanographic and Meteorological Controls on the North Sea circulation and hydrodynamics with a view to the Fate of North Sea Methane from well site 22/4b and other seabed sources

Janine Nauw[1], Henk de Haas[1] and Gregor Rehder[2]
[1] Royal Netherlands Institute for Sea Research, NIOZ, Texel, Netherlands, Janine.Nauw@nioz.nl & Henk.de.Haas@nioz.nl
[2] Leibniz-Institute for Baltic Sea Research, Warnemünde, Germany, gregor.rehder@io-warnemuende.de

Abstract

The North Sea hydrodynamics are key to the redistribution of methane released at site 22/4b, located at (57°55'N, 1°38'E) in the UK Central North Sea, 200 km east of the Scottish mainland. This review summarizes the current state of knowledge on the North Sea circulation, stratification and variability therein and briefly discusses the potential consequences for the distribution and fate of methane released from site 22/4b or other seabed sources.

Astronomical tidal waves follow an anti-clockwise path and tide-topography interaction generates a residual circulation in the same direction. Wind stress forcing can enhance, reduce or even reverse this circulation. Variations in the strength of the Fair Isle Current (FIC) are important. The FIC enters the North Sea between The Orkneys and Shetland, follows approximately the 100-m isobath, passes along site 22/4b, and ends up in the Norwegian Trench. The North Atlantic Oscillation (NAO) also causes variability. A positive (negative) NAO index is associated with stronger (weaker) than normal westerly winds. NAO+ situations strengthen the circulation in the North Sea, whereas it weakens during NAO- conditions and is directed northeastward. High positive correlations exist between the SST at site 22/4b and the NAO index. Climate change can have a long-term effect on the hydrodynamics of the North Sea.

Seasonal stratification has potentially the most important imprint on methane derived from well site 22/4b. Summertime heating stratifies the northern part of the North Sea. In autumn, loss of heat to the atmosphere causes the stratification to break down until tides and storms mix the entire water column. During the period of stratification, the bulk of (dissolved) methane released from site 22/4b gets trapped below the thermocline. The loss of methane to the atmosphere thus becomes a function of the relative time scales of transport and horizontal and vertical mixing processes versus the time scale of microbial degradation (oxidation) in the water column.

Introduction

Enhanced methane emissions to the atmosphere and the concomitant increase of the atmospheric methane inventory play a strong role in global warming due to its direct and indirect impact on the Earth's infrared radiation balance (IPCC , Working group I, 2013). The contribution of marine sources, including methane released at the seabed of shallow seas like the North Sea, to the atmospheric source strength is still highly uncertain (Judd, 2014; IPCC , Working group I, 2013). The prerequisite for marine geological sources to contribute to the total methane concentration of the atmosphere is to reach the surface mixed layer through turbulent mixing, advective transport, or partially uncoupled from water movement by rising gas bubbles. The latter process is considered the most efficient due to its potential to cross zones of reduced vertical mixing, e.g. regions with vertical stratification.

Natural Gas seepage of methane has been observed or inferred from observations at various sites in the North Sea [for instance Håvelsrud et al., 2012; de Haas and Shipboard Scientific Crew, 2011; Schroot et al. 2005]. In a multidisciplinary, quantitative approach, Schneider von Deimling et al. (2011) conclude, based on hydroacoustic, video, CTD and ROV sampling data and applying the gas bubble dissolution model of McGinnis et al. (2006), that of the 26 tons of methane released per year in the Tommeliten area, only about 4% reach the atmosphere directly as methane bubbles. However, they reason that the total methane flux from the seabed to the atmosphere is probably higher, since research cruises are mostly carried out during the fair weather summer period when the water column is stratified and methane can be trapped below the thermocline, as was also observed by de Haas et al. (2012). Rehder et al. (1998), who were the first to report on the blowout at well site 22/4b (Leifer and Judd, 2015; Schneider von Deimling et al., 2015), estimated that about 25% of the methane flux to the atmosphere from the open North Sea in May 1994 originated from site 22/4b, and also used the hydrodynamic model of Backhaus (1985) and Pohlmann (1996) to simulate the propagation of the dissolved gas in the water column. The hydrographic section presented in Rehder et al. (1998) shows a clear enrichment of methane below the thermocline in comparison to the concentrations in the mixed layer. This is consistent with various recent studies (Leifer and Judd, 2015; Schneider von Deimling et al., 2015; Sommer et al., 2015) all demonstrating that in the near field (some km) of site 22/4b – at least during the stratified season - more than 90% of the methane released by the blowout remains within below the thermocline.

This paper focusses on the hydrographic, hydrodynamic and atmospheric variations on time-scales from tidal to the long-term (future) climate variability locally at site 22/4b, which may have an impact on the methane flux from the sea bed and the amount that eventually reaches the atmosphere. The review will provide a review of hydrodynamic processes in the North Sea that affect the redistribution of methane released from a seabed source. These processes include tidal (residual) motion (steered by bathymetry), density driven currents and currents connecting the North Sea with the adjacent North Atlantic in the horizontal and the effect of seasonal stratification on the vertical exchange. Also atmospheric influences on current strengths and patterns and the variability of the seasonal stratification are reviewed, e.g. effects of the wind-stress forcing, the North Atlantic Oscillation and influences of climate change. Subsequently, we zoom in to the area around site 22/4b set into perspective the hydrodynamic time and length scales with our current knowledge of the lifetime of methane with respect to microbial turnover in the well-oxygenated water column. Comparing these time-scales essentially determine the chances for methane to reach the atmosphere under various hydrodynamic conditions.

Oceanography of the North Sea

2.1 Bathymetry

The North Sea is an epicontinental sea with a total surface area of 575,300 km^2 and a volume of 42,294 km^3 located on the northwest European passive continental margin, including the deep Skagerrak. The average water depth is 74 meters. The North Sea is only a small and shallow sea compared to the global ocean, the latter being 600 times larger and on average 50 times as deep. The small depth determines largely the oceanographic properties of this marginal sea. In the east and south it is bordered by the mainland of Europe (Norway in the north to France in the south) while it's western boundary is formed by the British Isles. In the south it is connected to the Atlantic Ocean through The English Channel. In the north it has an open connection to the Norwegian Sea. In the north the shelf break is located at about 200-m water depth. Maximum water depth in the southern North Sea is 40-50 m. Small depressions in the central and northern North Sea are of the order of 40 to 300 m deep. In the central North Sea a large shoal, the Dogger Bank, with a minimum water depth of less than 20 m is present (Figure 1). Furthermore, areas with tidal sand ridges, sand waves, tunnel valleys, iceberg grooves and other (post) glacial relic structures are present. The most striking morphologic feature of the North Sea however is the Norwegian Channel/Skagerrak. The Norwegian Channel is a large depression running north-south parallel to the Norwegian coast. In the north this depression is more than 400 m deep. In the south a sill exists, reducing water depth to about 280 m. South and southeast of this sill water depth increases to more than 750 m in the Skagerrak (Eisma et al. 1979; Otto et al., 1990). The interaction of tidal waves and topography causes a tidal residual circulation patterns along isobaths (see section 2.2).

2.2 Tides and tidal (residual) circulation

The most dominant tidal components in the North Sea are the semi-diurnal lunar tide, M2, and the semi-diurnal solar tide, S2. These have a period of 12:25 hours and 12 hours, respectively. Figure 2a shows the amplitude and the phase of the M2-tide in the North Sea (Egbert et al., 2010) and is slightly different from the one given in Otto et al. (1990). The most northern amphidromic point is located close to Norway. The tidal wave enters the North Sea from the North Atlantic and travels along the British coast and proceeds around the two amphidromic points along the Dutch, German and Danish coast, leaving the North Sea along the Norwegian coast again. The tidal wave also enters from the south west, through the English Channel. In the Irish Sea the wave enters from the south. The influence of bottom friction is clearly visible by the decrease of tidal amplitude along its path.

Interaction between the M2 and S2 components generate the 14-day spring-neap tidal cycle. The other astronomical components can be found in Pugh (1987) and Hoitink et al. (2003). Non-linear interaction between tidal components due to advection and friction generate long-term averaged values or residuals (Figure 2b) and compound tides. Of these the M_4 is perhaps the most important in the North Sea (Egbert et al., 2010).

Besides causing the tidal residual circulation due to interaction with the local bathymetry, tides also induce turbulent mixing (Ridderinkhof and Zimmerman, 1992; Simpson, 1998; Zimmerman, 1986) and are therefore important for the dispersion of dissolved or suspended material in the North Sea.

Tidal and residual currents are strongly modified by local bathymetry. To first order, the tidal wave follows bathymetry and in second place, tide-topography interaction can cause a residual current along the lines of equal water depth, if there is a small amount of dissipation (for instance due to bottom friction). Some 40 km to the southwest of site 22/4b, at the Forties field, the British Geological Survey have done detailed measurements about the local current conditions (Graham, 1985). Currents at the latter location are orientated predominantly south to north and have a maximum value of 55 cm/s to the North and 36 cm/s to the South at a depth of 52 m; the difference between these values indicates a

northward directed residual flow in the order of 20 cm/s (Figure 3a,b). Tidal currents from the Oregon State University (OSU) Tidal Inversion Software (OTIS, Egbert et al., 2010) have an M2 tidal amplitude of 26 cm/s at that location, but with the same orientation at the forties site. This model predicts a similar tidal flow near site 22/4b even though the local bathymetry at site 22/4b is more oriented southwest to northeast (Figure3c). The latter may have some influence on the orientation of the residual currents.

2.3 Connection with the North Atlantic

The circulation in the North Sea is also determined by the inflow of saline Atlantic water through the northern entrances and (to a lesser extent) through the English Channel. Oceanic water from the northern North Atlantic Ocean follows three paths of persistent inflows into the northern North Sea: the Fair Isle Current (FIC), the inflow along the western edge of the Norwegian Trench (Slope Current, SC) and the East Shetland Atlantic Inflow (ESAI), offshore of the FIC (Turrell et al., 1996 and Figure 4). The ESAI is particularly persistent during the summer months. Substantial salinity changes have been observed in the northern North Sea, which could be related to a decadal variability of the two western North Sea inflows, the FIC and the ESAI. Site 22/4b is located at 57°55'N, 1°38'E within the FIC on the 100 m isobaths, slightly south of the ESAI. The Atlantic inflow displays a seasonal variation with maximum inflow during winter months. The minimum inflow during the summer correlates with a salinity maximum in the waters at the shelf edge.

The FIC was identified in the JONSDAP76 experiment (Dooley, 1983) and has been extensively investigated during the Autumn Circulation Experiment (ACE, from 18 September 1987 to 5 January, 1988; Klein et al., 1994; Turrell and Henderson, 1990; Turrell et al., 1990; Turrell et al., 1992) and the Nord Rand (NORA, northern boundary, from 15 July to 21 August, 1990 by Klein et al., 1994) experiment. Note that there is some debate on the name of the topographically steered eastward flowing current in the central northern North Sea. The current indicated as the FIC in Figure 4, is often referred to as the Dooley Current (DC, Svendsen et al., 1991; Klein et al., 1994; Winther and Evensen, 2006). Moreover, in sketch of the current structure in Hill et al. (2008) a relation between the ESAI and the Dooley Current is suggested. Here we follow Turrell et al. (1996) and Figure 4 and refer to the current following the 100 m isobaths as the FIC. In autumn, the FIC is a homogeneous current with a salinity of 35.05 to 35.15, having a stable mean residual current with a magnitude of about 10 cm/s within the North Sea (Turrell et al., 1990). The mean transport through the FIC was ~0.13 Sv (1 Sverdrup = $1.0 \cdot 10^6$ m^3/s) and comparable with the estimates of 0.3 Sv (Dooley and Furnes, 1981) and 0.26 Sv (Klein et al., 1994). A seasonal change was observed varying between ~0.4 Sv during the late summer and 0.15 Sv during the winter months in the ACE project.

Daily mean current transports in the FIC appear not to be correlated with daily mean winds as the response of the FIC to the mean wind alters with the changing stratification over the measurement period. In October, when stratification was present (see: 2.4 Climatology and seasonal stratification), transport seems to be enhanced (reduced) by North North Westerly (South South Easterly) winds blowing directly along the mean topography (see: 2.7 Wind-driven circulation). In November, when stratification is decaying, westerly winds appear to strengthen the current, where SSE winds still reduced the currents. In December, winds from the southwest produced the strongest currents and the absence of the wind lead to a small reversed transport (Turrell et al., 1990).

The tidal current strength in the central part of the FIC varies between about 20 cm/s during neap tide and 50 cm/s during spring tide and reaches almost all the way to the bottom (Klein et al., 1994 and Figure 5). In Figure 5, the FIC is located at N1 (59° 0.16' N, 1° 59.85' W) and N2 and (59° 0.10'N, 1° 0.30'W) and thus to the North West of site 22/4b and upstream with respect to the predominant path followed by the FIC. The tidal current strength during spring tide is similar to the maximum observed currents of 55 cm/s at the forties site in Figure 3a,b.

Figure 6 shows estimates of the total inflow from the North Atlantic into the Northern North Sea between the Orkneys and Norway (ICES, 2005). This flux is thus composed of the inflow due to the FIC, ESAI, the SC and the Norwegian Coastal Current (NCC, introducing a negative contribution). These are based on the results from a numerical model (ICES, 2005). The time-series show significant annual variations with an average volume flux of 1.2 Sv towards the south. Between 1988 and 1995 a significantly stronger inflow of nearly 1.5 Sv was estimated in the model.
In the south the North Sea is fed by oceanic transports from the English Channel. The estimated water flux through the channel is 1 to 2 Sv (du Bois et al., 1995). English Channel water predominantly follows the European continent and, based on radioactive tracer measurements, it is estimated that it takes about 170 – 250 days for this water to reach the northern part of Denmark.
In the Skagerrak, North Sea water leaves the domain along the Danish coast. Estimates are about 0.2 Sv (Otto et al., 1990) and 0.05 Sv (Rydberg et al., 1996). The flow of surface water from the Kattegat is estimated at 0.05 -0.06 Sv by Andersson and Rydberg (1993), which contains about 0.015 Sv freshwater, mainly from rivers in the Baltic. Geostrophic transport estimates varied from 0.26 to 0.4 Sv inflow and 0.64 to 0.0 Sv outflow based on the SKAGEX data set (Danielssen et al., 1997; Skogen et al., 1997). Figure 7 shows a schematic representation of the circulation in the Skagerrak from Danielssen et al. (1997). Note that the maximum latitude in Figure 4 is 6^{o}E and thus matches perfectly to the western part of Figure 7. Apparently, what is called the ESAI in Figure 4 is fed into the Atlantic Water deep, AW^{d}, in Figure 7. Moreover, the FIC in Figure 4 feeds the Atlantic Water upper, AW^{u}, in Figure 7. Therefore a residual transport path between site 22/4b and the Skagerrak exist, even though that does not necessarily mean that substances released at site 22/4b will be transported to the Skagerrak, as high-frequency variability induced by tides, wind-driven and density-driven circulation will transport substances in other directions.

2.4 Climatology and seasonal stratification

A new improved climatology of temperature and salinity on the European Shelf is given in Berx and Hughes (2009) on near bottom and surface values based on data between 1971 and 2000. It is an improvement to the Janssen et al. (1999) climatology based on data between 1900 and 1996. Overall a minor temperature increase is observed between the Janssen et al. (1999) and the Berx and Hughes (2009) climatology, which is due to the fact that the period 1997-2000 was much warmer than the average over the entire 30-year period and possibly related to a regime shift between 1982-1988 (Beaugrand, 2004). Figure 8 shows the annual cycle of temperature for the near-surface and near-bed levels derived from a harmonic analysis method of least squares (HAMELS, Emery and Thomson, 1997). The temperature decreases with latitude and the influence of the North Atlantic Ocean is clearly visible in the northern part of the North Sea. The largest seasonal variations occur in the southern part of the North Sea and the German Bight, where the shallower regions are located. In the northern part of the North Sea, the amplitude of the seasonal variation of temperature in the near-bed layer is only small, indicating the separation of the lower layer from the upper layer during the summer stratification in this area. In this area tidal currents are relatively weak (see also Figure 3) and not able to mix the input of buoyancy from (summer) solar heating down (Bowers and Simpson, 1987).
The salinity distributions (Figure 9) show that waters close to the North Atlantic are more saline. Moreover, the highest amplitudes in surface salinities are observed in the regions of fresh water inflow (ROFIs), especially in the Baltic outflow region. The seasonal cycle in the salinity is caused by a changing balance in precipitation minus evaporation and variations in land and river runoff. Besides a seasonal cycle, there is still ample of irregularity in these parameters, which makes it difficult to identify the seasonal cycle in the salinity distributions and which is represented by the low R^2. A clear seasonal cycle can be identified only in the Baltic outflow, where maximum surface salinities are observed between September and December and minimum surface salinities in the period between April and June,

following a maximum freshwater outflow from the Baltic from February till March (Hordoir and Meier, 2010). The Sea Surface Salinity (SSS) near site 22/4b is determined by the inflow from the north and is about 35 PSU, the annual amplitude is only small: less than 0.4 PSU. The maximum salinity occurs mid-winter. Near the bed the salinity is also about 35 PSU and the annual variability equally small as near the surface. There, the salinity also attains its maximum in the middle of the winter.

At the transition between fully mixed waters and stratified waters, mixing fronts occur. The locations of these tidal mixing fronts are shown in Figure 10. A balance between tidal and wind-driven mixing and thermal heating leads to the creation and destruction of seasonal tidal mixing fronts between well-mixed and stratified waters. The location of the tidal mixing front is usually determined for the entire summer season (June-July-August) and is defined as the location of the surface to bottom temperature difference being +0.5^{o}C (Holt and Umlauf, 2008; O'dea et al., 2012). The resulting front shows reasonable agreement with a rough estimate of the location identified in earlier days by Pingree and Griffiths (1978) based on a measure of the ratio of rate of production of potential energy to the rate of tidal energy dissipation leading to a relation proportional to ~ $h/(C_D|u|^3)$, where h is the bathymetry, C_D the drag coefficient and u a measure for the velocity. This leads to a frontal position located in the southern part of the North Sea between the central part of the UK, crossing the North Sea to the Netherlands, more or less following bathymetry at about 50 km offshore towards Denmark. For the purpose of this review with a focus on site 22/4b, the location of the mixing fronts was determined using the Berx and Hughes (2009) climatology for each month (Figure 10). Already in April, site 22/4b is surrounded by a tidal mixing front, suggesting that the water column in this area is already stratified. The stratified area is already expanded in May to its mean 'summer' location and the Celtic Sea front, the front west of Scotland and the North Sea front become apparent. From September onwards the North Sea tidal mixing front retreated back to Norway and almost surrounds site 22/4b in November.

The seasonal variability of the sea surface and near bed temperature and salinity at site 22/4b derived from Berx and Hughes (2009) is shown in Figure 11. The sea surface temperature (SST) has a minimum of 5.9^{o}C in March and increases due to solar insolation until it reaches a maximum of 13.8^{o}C in August. The near bed temperature also has a minimum of 5.9^{o}C in March, when the water column is vertically well-mixed, after which the seasonal thermocline develops as seen by the difference in temperature between the surface and the bottom. The bottom temperature then slowly increases to a maximum of 8.9^{o}C in November due to vertical turbulent mixing across the stratification and horizontal advection. Then the temperature difference between surface and near bed decreases significantly as the stratification breaks down again. The sea surface salinity (SSS) shows an inverse behavior compared to the SST as relatively fresh waters from high runoff from the Scandinavian Peninsula reach the site in July leading to a minimum SSS of 34.82 in July. Maximum of 35.07 SSS are observed in January. Near bed salinity follows the behavior of the SSS in the non-stratified period and remains fairly constant during the period of seasonal stratification and returns back to its highest value of 35.14 in November.

During the PROVESS (Processes Of Vertical Exchange in Shelf Seas) experiment the start of the autumnal erosion of the thermocline was investigated (Howarth et al., 2002). The experiment took place at two contrasting sites in the North Sea, one in Dutch coastal waters and one in the Central part of the Northern North Sea at 59^{o}20'N and 1^{o}E, where local water depth is 110 m, between 5 September and 9 November 1998. However, the actual breakdown of the thermocline did not take place before the beginning of December 1998 as demonstrated in a 1D numerical simulation (Bolding et al., 2002). Vertical exchange processes cause the erosion of the thermocline and are controlled by turbulence characteristics. As a consequence, the timing of the autumnal breakdown in stratification is directly related to the vertical heat flux driven by turbulent mixing across the thermocline. Turbulence is generated at the surface by wind and (breaking) waves and at the sea bed by bottom friction. At the interface between the surface and bottom mixed layer, turbulence levels are reduced and vertical fluxes are small, except under certain conditions. For instance, vertical fluxes can be generated by internal

waves breaking at the interface, when generated by tidal flows forced over topography (Rippeth, 2005; van Haren et al., 1999) or shear generation across the interface by inertial currents following a strong wind forcing event (Knight et al., 2002; MacKinnon and Gregg, 2005; Rippeth et al., 2005; van Haren, 2000). Periods of enhanced shear can lead to shear instability and diapycnal mixing as the system appears to be only marginally stable (van Haren et al., 1999). In periods with seasonal stratification, the shear between the layer above and below the thermocline rotates in clockwise direction at the inertial period. Shear is enhanced in periods when the wind stress, the (mostly tidally driven) bed shear stress and the shear vector are aligned, causing enhanced levels of mixing (Burchard and Rippeth, 2009). The strength of the turbulence therefore depends on the local water depth, tidal current strength, stratification, bed roughness, wind stress and waves. Orbital velocities associated with the latter appeared to be negligible at the PROVESS site in the northern North Sea due to the large water depth of 110 m (Burchard and Bolding, 2002). Besides these vertical processes, horizontal advection of Atlantic water may also impact the stability locally (Bolding et al., 2002; Burchard and Bolding, 2002). During the PROVESS campaign, however, tidally and (wind-driven) advective transports were negligible (Luyten et al., 2002). The PROVESS site is only about 160 km NNW of site 22/4b and has a similar water depth, therefore processes causing vertical exchange will likely be comparable at both sites, implying a similar seasonal cycle in terms of stratification and destratification (see Figure 10). The only main difference between the two sites is the presence of the FIC at site 22/4b, and hence non-negligible advective transports and the presence of the bubble momentum plume itself, causing additional vertical motion, which may cause an early breakdown of the thermocline (Nauw et al., 2015).

2.5 Variability in thermocline structure

The temperature of the North Sea is mainly controlled by local solar heating and heat exchange with the atmosphere. A balance between tidal mixing and local heating introduce the development of a seasonal stratification from April/May to October/November in the northern parts of the North Sea. The annual cycle of Sea Surface Temperature (SST) in the North Sea (Figure 12) shows highest temperatures in late summer (August) and lowest temperatures in February. Also, significant interannual variations can be observed, with highest summer temperatures in 2003 and 2004. These positive SST anomalies started in June 2001 and ended in March 2005 (ICES, 2005). The temperature of the upper layer of most of the North Sea was between 0.5 and 1.5^{o}C warmer than normal, which is defined as the long-term average during the period 1971-2000. The exception is the western Norwegian coastal water, which was close to normal during the first half year.

The annual mean temperature and the salinity anomalies of the FIC (Figure 13) show strong interannual to decadal variability. Moreover, higher than normal temperatures appear to be correlated with higher than normal salinity anomalies (and vice versa). Temperature and salinity anomalies may therefore induce a year-to-year variation in the stratification and thereby changes in the density driven circulation (see Density Driven Circulation) at the location of site 22/4b, which is located in the center of the FIC. Spatial and temporal variations in the thermocline structure can be expressed in terms of thermocline depth, intensity, extension and first day of the year on which a noticeable thermocline is observed. These variations are difficult to observe in the field; therefore Meyer et al., (2011) demonstrated these in a 60-year long hindcast using the Hamburg Shelf Ocean Model (HAMSOM). The thermocline depth is defined where the vertical temperature gradient exceeds 0.1^{o}C/m and thermocline intensity is defined as maximum vertical temperature gradient. If one defines the thermocline as being developed when its horizontal extent exceeds 10.000 km^{2}, then the thermocline in the North Sea usually develops early April. The mean thermocline depth in the model showed considerable seasonal and interannual variability between 7.5 m up to more than 40 m. A trend could be found neither in the thermocline depth, nor in the thermocline intensity, being between 0.1 and 0.4^{o}Cm^{-1}. This suggests that the observed

warming in the 1980s affected the entire water column without influencing the thermocline structure (Figure 14).

2.6 Density-driven circulation

During the summer and autumn months, when (part of) the North Sea is stratified, the density-driven component adds a significant contribution to the residual current. Under stratified conditions, mixing is reduced at the thermocline, effectively decoupling the upper layer from the lower layer. In contrast, well mixed areas remain in particular in the shallower parts of the North Sea, where tidal mixing is sufficient to overcome the input of potential energy from summer heating. Locally, at the tidal fronts separating stratified from well-mixed areas, sub-surface along frontal jets with speeds in the order of 2-16 cm/s are generated (Brown et al., 1999; Simpson and Pingree, 1978; van Aken et al., 1987); cross-frontal velocities of 4 cm/s have been observed (Hill et al., 1993; Matthews et al., 1993). The cross-frontal residual current shows convergence at the surface and divergence near the bottom and is about one third of the strength of the jet in the along frontal direction (Lwiza et al., 1991). In general, these frontal jets are small-scale, having a width of 10-20 km and a near-surface current with velocities in excess of 0.1 m/s in the direction with the cold bottom pool water to the left (Brown et al., 1999). The tidal currents near the bottom lead those near the surface on both sides of the front, whereas in well-mixed conditions the phase change is gradual.

The tidal current vector rotates clockwise in the upper part of the water column and anticlockwise in the bottom layer. An explanation for this is related to the different thickness of the frictional layers for the clockwise and anticlockwise component, which described the ellipse-shaped tidal current vector (Maas and van Haren, 1987; Souza and Simpson, 1996; van Haren, 2000). A more subtle feature is the observed clockwise veering of the semi-major axis with depth from the surface (Lwiza et al., 1991).

Despite the relatively large distance of tidal fronts from site 22/4b and most natural gas seepage sites in the North Sea, cross-frontal circulation may be important for the transport of methane from a source in a stratified region to a well-mixed region and create a pathway for exchange with the atmosphere (see section 3.2).

The purely density-driven seasonal circulation was determined using POLCOMS (Proudman Oceanographic Laboratory Coastal Ocean Modeling System) by Holt and Proctor (2008). This model is well capable of reproducing the seasonal behavior of the hydrodynamics of the northwest European Shelf (Holt and Umlauf, 2008). The location of quasi-geostrophic jet characteristic for the tidal mixing fronts compared well with drifter observations (Hill et al., 2008) and that one of the fronts is located near the site 22/4b (Figure 15). The associated frontal jets form transport pathways for dissolved and suspended material. Moreover, fronts themselves are associated with higher productivity, likely due to cross-frontal exchange of material, either related to a cross-frontal circulation or due to intrinsic instabilities leading for instance to the formation of eddies (Badin et al. 2009; Le Boyer et al., 2009).

2.7 Wind-driven circulation

The weather across the North Sea is dominated by westerly winds. The classical presentation of the circulation in the North Sea is described by an anti-cyclonic gyre driven by wind-stress forcing and non-linear tidal interaction. However, Kauker and von Storch (2000) applied an atmospheric forcing by the ECMWF reanalysis from 1979 to 1993 to an ocean general circulation model. They found that the resulting circulation in the North Sea is dominated by two circulation patterns. One displays the great gyre circulation, which can be either clockwise (15% of the time, right panel of Figure 16) or anti-clockwise (30% of the time, left panel of Figure 16). The anti-clockwise circulation is excited by southwesterly winds (left panel Figure 17), whereas northwesterly winds cause a clockwise circulation (right panel of Figure 17) winds. The other circulation pattern has a bipolar structure with a counter rotating flow in the northern (top panel of Figure 16) and southern (bottom panel of Figure 16) part of

the North Sea and occurs 45% of the time, corresponding to southerly (bottom panel of Figure 17) and northerly (top panel of Figure 17) winds. Moreover, during 10% of the time, the circulation in the North Sea even halts, corresponding with weak winds (central panels of Figures 16 and 17).
This implies a southwestward directed contribution by the wind-driven residual circulation at site 22/4b during southwesterly and easterly winds (left and right panels in Figures 16 and 17) and a northeastward directed contribution during periods with predominantly southerly winds (top panels in Figure 16 and 17) and no significant contribution under all other dominant wind conditions.

2.8 Climate variability

Especially, during winters the average pressure system over the North Sea is controlled by a large scale system over the North Atlantic, consisting of a low pressure area over Iceland and a high pressure area over the Azores. The associated westerly winds blowing across the North Atlantic bring moist air into Europe and over the North Sea. Variability in the wind speed and direction, however, is strong. The most prominent influence is from the North Atlantic Oscillation (NAO), which is related to the strength of the westerlies, which varies on a decadal frequency (Hurrell, 1995). The winter (December through March) NAO index is defined as the normalized sea level pressure (SLP) difference between Lisbon (Portugal) and Reykjavik (Iceland). Figure 18 shows the NAO index for the period 1864 until 2014 (http://climatedataguide.ucar.edu/guidance/hurrell-north-atlantic-oscillation-nao-index-station-based). The black line shows the five year moving average. Fluctuations between a positive and negative NAO index on the decadal frequency are apparent. A positive (negative) NAO index is associated with stronger (weaker) than normal westerly winds. In years when westerlies are strong (corresponding more-or-less with wind pattern in the left panel of Figure 17), summers are cool and winters are mild and rain is frequent. In periods with weak westerlies (corresponding more-or-less with wind pattern in the right panel of Figure 17), temperatures over Europe are more extreme both in summer and in winter, heat waves and deep freezes occur more often and the weather is characterized by reduced rainfall.
Between the years 1950 to 1970 a negative NAO prevailed, whereas the NAO was strongly positive in the years 1980 to 2000. The sea-surface temperature (SST) response of the North Sea to negative and positive NAO conditions is examined by Pingree (2005). The response to a changing NAO is estimated to be about 5 months. This comprises of the wind-induced inflow, the shelf circulation and the local climate forcing. Under marked positive NAO conditions, associated with strong North Atlantic wind induced inflow, mean temperatures in the North Sea are about 1^{o}C warmer than under negative conditions. In 1996, the NAO was extremely negative, causing the North Sea wind-driven circulation to be halted.
A significant correlation is found between the spring NAO value and the wind stress. The relation is not significant between spring NAO values and the spring air temperatures. Thus the NAO can directly influence the timing of stratification through changes in the spring wind stress (Sharples et al., 2006). In Reid et al. (2003), high or positive NAO index conditions were associated with strong inflow and transport through the North Sea and weaker flows were associated with negative NAO anomalies. Changes in the NAO are correlated with changes in the strength of the North Atlantic Current (NAC). The correlation is maximal with a lag of about 6.5 months. Variations in NAO explain 67% of the total variance in the NAC (Pingree, 2005).
Plag and Tsimplis (1999) found coherent temporal variability in the annual and semi-annual constituents in sea level, air pressure, air temperature and the wind field over northwestern Europe on decadal scales. Based on the patterns of these climatological variables, North-western Europe can be clearly separated into a continental and maritime area separated by an intermediate zone, which for annual component of the air pressures at sea level is roughly aligned to the Dutch/German North Sea straight across the Baltic Sea ~ through points (10^{o}W, 47^{o}N) and (30^{o}E, 60^{o}N). The position of this intermediate zone apparently slightly shifted northwestward in the late 20th century. The sea level variations on decadal scale are closely correlated with the atmospheric forcing. The variation in seasonal air pressure

may be linked to variations of the North Atlantic Oscillation on decadal time scales and a general warming trend over Europe.
A warming trend has been observed in the North Sea. Becker and Pauly (1996) investigated sea surface temperature changes in the North Sea and their causes. Based on a 25-year time-series of patterns of sea surface temperature (SST), Becker and Pauly (1996) came up with the eight different regions in Figure 19a, which closely resemble the ICES boxes for North Sea water masses given in Figure 19b and also the distribution in hydrographical regions given in Otto et al. (1990). The approximate location of site 22/4b is indicated with a red dot in box 7 in Figure 19a and in box 2 in Figure 19b. In the ICES boxes distribution a clear relation is shown with the currents between the Faroe and Orkney islands.
In Becker and Pauly (1996), it was shown that the oceanic influence in the northwestern part and the continental influence in the northeastern part are clearly reflected in the different SST behavior. Positive SST anomalies usually start in the Southern Bight and move with a delay of several weeks into the central and northern North Sea. No temperature trend was observed in either of the boxes in the period between 1969 and 1993. High correlations between SST anomalies and the NAO index were expected in regions 1 and 5, but the contrary was found (Figure 20). Apparently, SST anomalies in the Southern Bight are independent of the North Atlantic Atmospheric Circulation. However, a distinct correlation was found between the NAO and the SST time series with highest correlations in the central northern part of the North Sea (region number 7). Site 22/4b is close to the location of the highest correlations and thus the SST at this site is strongly influenced by the NAO. Here, it is likely that the SST is dominated by air-sea exchange, which is obviously closely related to atmospheric forcing and weather patterns.
The wind-driven residual circulation in the North Sea is significantly influenced by the North Atlantic Oscillation (NAO). This can be seen in Figure 21, which shows results from a model calculation by Sündermann and Pohlmann (2011) indicating that the currents under a NAO+ situation are much stronger than during a negative one. Moreover, currents in the central northern part of the basin, where site 22/4b is located, are directed eastward under NAO+ conditions and northwestward under NAO- conditions, which obviously influences the spreading of (passive) tracers, such as methane (strictly speaking, the dissolution of methane causes a slight reduction in seawater density (O'Sullivan and Smith, 1970; Schmid et al., 2004), which however can be neglected due to the small solubility of methane in seawater (Gupta, 2010; Linke et al., 2010). The results shown in Figure 19 confirm the results of Kauker and von Storch (2000), where strong westerlies (correlated with NAO+) induce a counterclockwise rotating circulation, strengthening the residual counterclockwise circulation. And weak westerlies (or easterlies, which are correlated with NAO-) induce a clockwise circulation, thereby opposing the tidal residual circulation.

2.9 Climate change

Temperature and salinity show significant annual, interannual and decadal variability (Becker and Pauly, 1996; Sündermann et al., 1996). Two relatively sudden climate changes have been observed in a wide-scale and rather sudden change in plankton, benthos and fish populations, and stand out as exceptional (e.g. Kirby and Beaugrand, 2009; Weijerman et al., 2005). The first change occurred in the late 1970s, and was distinguished by a reduced inflow of Atlantic water and cold-boreal conditions (Reid and Edwards, 2001). Between 1989 and 1994, oceanic inflow increased markedly, as did sea surface temperature (Beaugrand, 2004; Reid et al., 2001) and the heat content (Pohlmann, 1996).Changes in hydrological and meteorological variables clearly show a switch in the 1980s. Salinity dropped significantly and the westerly winds and north hemisphere temperatures increased. An example of the increasing seawater temperatures is given in Figure 22, which shows observations of the temperature at Arendal on the Norwegian Skagerrak coast (ICES, 2007). The temperatures in the autumn of 2006 remained above average, sometimes even above the 2 standard deviations (SD) line.

The low NAO index in the 1960s coincided with the “Great salinity anomaly”, which was a low salinity pattern propagating in the North Atlantic (Dickson et al., 1988; Mork and Blindheim, 2000). The anomaly arrived in the North Sea in the late 1970s and induced pronounced minima in the salinity and temperature. It was first observed in the Rockall channel in 1976 and later in the northern and central North Sea, in 1977/1979 (Becker and Pauly, 1996). During the latter period, the SST anomaly in the North Sea was markedly negative. In 1989/1990 a high salinity anomaly was connected with a positive temperature anomaly in the North Sea (Becker and Dooley, 1995). Pohlmann (1996) shows that the interaction between wind stress and thermal forcing is the main cause of the heat content variability. Temperature anomalies in 1988-1992 were high, suggesting a trend. However, these occurred in the end of his simulation and Becker and Pauly (1996) suggests that the temperature increase might be a temporal anomaly similar as in the 1970s.
In the future, air temperatures over the North Sea are expected to increase by 2 °C to 3.5 °C by the 2080s, with high summer temperatures becoming more frequent and very cold winters becoming increasingly rare (e.g. Hulme et al., 2002; van den Hurk et al., 2006). Modelling studies suggest that future climate change will lead to a further increase of SST by 1.5 to 4 ^{o}C and a further decrease of the Sea Surface Salinity by ~0.2 PSU and strengthens the stratification by 20% and that stratification start approximately 5 days earlier and breakdown occurs 5-10 days later, thereby increasing the period of stratification in climate predictions for 2070-2098 with the SRES A1B scenario (Ådlandsvik, 2008, Dye et al., 2013; Holt et al., 2010, Nakicenovic and Swart, 2000l Mathis and Pohlmann, 2014). In a discussion paper by Holt et al. (2014) an overview is provided on how climate change can affect the strength and duration of the seasonal stratification in shelf seas. Changes in the summer stratification are set by the difference in seasonality of the heat flux and not by the increased heat flux itself. The bottom layer temperature in summer is essentially determined by temperatures of the well-mixed water column in spring and the surface temperature is determined by summer heat flux. Hence, only relative changes in the summer and winter/spring warming lead to changes in the thermal stratification. However, if the entire water column increases by the same temperature, the non-linearity in the equation of state leads to a larger density difference between the upper and the lower layer. Using climatological temperature and salinity data from Berx and Hughes (2009), the maximum density difference is 1.7 kg/m^3 occurring in August; adding 1.5^{o}C (taken from Fig. 4 in Mathis and Pohlmann, 2014 at the site 22/4b) to the near-surface and near-bed climatological temperatures and leaving the salinities values the same leads to a maximum density difference of 1.8 kg/m^3, e.g. and increase of 6%. Besides temperature, changes in evaporation minus precipitation can be important in changing the stratification. Increased (decreased) wind speed in spring may delay (hasten) the onset of stratification, whereas it may cause an early (late) breakdown of the stratification in autumn. The location of tidal mixing fronts, separating well-mixed from seasonally stratified areas may be affected by changes in wind speed and direction, if the positions are only weakly constrained by tidal mixing and bathymetry. An intensification of the frontal jets and associated baroclinic eddies (Badin et al., 2009) is expected as shallower waters warm faster than deeper ones (Holt et al., 2012). The duration of the seasonal stratification has implications for the dispersion of dissolved methane in the lower layer and will be subject of the next section.

Relevant Time scales

Whether the methane released at site 22/4b actually reaches the atmosphere is essentially based on the time scales of horizontal and vertical mixing depending on the hydrodynamics. Large time-scales involved in vertical mixing under stratified conditions hamper the direct transfer of dissolved methane to the atmosphere. In the dissolved state, oxidation of methane can prevent the exchange with the atmosphere completely and introduce the methane into the biogeochemical cycle. In the following two sections the relevant hydrodynamic and oxidation time-scales are summarized and put into perspective.

3.1 Hydrodynamic Time scales

Several studies have calculated the flushing timescale of the ICES boxes as shown in Figure 17b. The flushing time scale is defined as the volume of such a box divided by the gross flux through the boundaries of the box. Hence, the flushing time is the period in which the volume of a selected box is completely refilled with water from outside of that particular box. For this study we are primarily interested in box 2 (Figure 19b) of which the flushing time scales are summarized in Table 1. Clearly, values vary strongly between studies, where the value by ICES (1983) and Prandle (1984) appear to be an overestimate, which in the case of the former is attributed to a lack of in-situ observations. In all other (model) studies the flushing time scale appears to be in the order of one month (varying between 9 and 50 days). Thus within about a month the complete water mass in ICES box 2 is replenished.

The residence time indicates the time needed to transport a substance from a certain position to the boundaries of a chosen domain and thus related to the travel times of radioactive material as in Prandle (1984). However, similar as the flushing time, also the residence time is probably an overestimate in the latter study. Blaas et al. (2001) show that the residence time of water in the North Sea is significantly reduced due to tidal stirring and density driven circulation. Based on their results, the residence time of substances released at site 22/4b is in the order of one year, indicating that after a year the substance released there is no longer present in the North Sea.

Tidal excursion length is the net horizontal distance travelled by a water particle from low water slack to high water slack or vice versa. It gives an indication of the movement of substances within the water parcels during one tidal cycle. It can be used to describe the movement of pollutants in estuaries during a tidal cycle and is defined as $E=U_0T/\pi$, which is essentially derived from integrating a sinusoid with an amplitude of U_0 over half of a tidal cycle with a period T (Thomann and Mueller, 1987). With T=12 hours and 25 minutes (M2 tidal period) and a tidal amplitude U_0=25 cm/s (Nauw et al., 2015), the tidal excursion becomes 3.3 km. Thus a water parcel released at site 22/4b travels 3.3 km away from the site before returning back. However, in this period it was subjected to the residual background current of the same order of magnitude induced by the presence of the FIC, leading to a distance travelled of $U_0T/2$=5 km, significantly larger than the tidal excursion.

In well-mixed areas/periods in the North Sea, the combined mechanisms of tidal stirring, wind-driven mixing and/or convection will remove vertical gradients in the temperature or salinity caused by warming/cooling at the sea surface or advection of fresher/more saline waters. An estimate of the timescale associated with this process is $T=H^2/K_z$~1 to 12 days using water depth of 100 m and a vertical diffusivity, K_z, between 0.01 and 0.1 m^2/s as shown in the well-mixed lower and upper part of the eddy diffusivity profiles in Bolding et al. (2002) and Luyten et al. (2002) for measurements at the PROVESS site. This range for the vertical diffusivity corresponds with that given by Simpson and Sharples (2012) for the bottom layer of a tidally energetic shelf region. It is larger than the range suggested for the wind-mixed surface layer, being 10^{-4} to 10^{-2} m^2/s in Simpson and Sharples (2012), which would lead to time-scale larger than 12 days. Turbulent mixing processes act in the same way on the vertical dissolved methane concentration distribution as on the water parcels and will cause transport from the seafloor to the surface on a timescale in the same range as the period for flushing of ICES box 2, suggesting that the release of methane to the atmosphere occurs in or near to the surface area of that box.

In stratified areas/periods, time-scales involve mixing across the front both in the horizontal and the vertical direction. Seasonal tidal mixing fronts are suggested to act as a barrier against the transport of contaminants as locally at the frontal position the mixing in inhibited (Hill et al., 1993). However, the frontal system itself generates a circulation locally at the position of the front as already discussed earlier. The along-frontal jet is in near geostrophic balance and has velocities in the order of 15 cm/s. Cross-frontal secondary circulation is smaller and ~5 cm/s, which leads to a timescale of 0.5 to 1 day with a width of 2 km (Hill et al., 1993) to 4 km (van Aken et al., 1987). Along-frontal and cross-frontal

diffusivities were estimated to be 80 m^2s^{-1} based on behavior of buoys in a frontal area near the British coast. The Lagrangian length scale associated with these motions is 1 km and the time scale 5-9 hours (Hill et al., 1993). These diffusivities (this time-scale) seem(s) a bit too large (small) compared to the time-scale related to the cross-frontal circulation. The frontal system can become baroclinically unstable, leading to the formation of meanders with a wavelength of ~10 km and may shed eddies with the size of the internal Rossby radius of deformation. Such eddies may promote mixing across the front (Pingree, 1978); time-scales of eddy-induced diffusion was estimated to be about 2-3 days based on sequences of cloud-free images (Simpson et al., 1981) and drifter tracks (Badin et al., 2009). The density-driven flows themselves transport material, contaminants and any dissolved compound like dissolved methane in the along- and across-frontal direction.

Moreover, these density flows seem to coexist with inertial currents generated by wind events. Inertial currents cause a sheared flow across the thermocline and locally enhance mixing. The transit time for the ~500 km long front from the Firth of Forth to the Doggerbank following the 40m isobaths is approximately 80 days with a conservative estimated of the frontal speed of 7.5 cm/s (Brown et al., 1999). van Aken et al., 1987) showed jet-like structures with flows in excess of 10 cm/s increasing to 15 cm/s after a period with strong winds and subsequent cooling of the sea surface, which caused a displacement and strengthening of these structures. A density-driven tidal front was also observed near the 22/4b site (Hill et al., 2008; Nauw et al., 2015).

Vertical mixing across the thermocline adds another time-scale to the variability. Heat from the surface layer is mixed down into the deeper layers through molecular diffusivity of heat, which is $\nu_T=10^{-5}$ m^2s^{-1}, which falls within the range of typical values of the eddy diffusivity within the thermocline of $K_z=10^{-6} – 10^{-4}$ m^2s^{-1} indicated by Simpson and Sharples (2012) and Luyten et al. (2002) and $K_z=4.0\cdot10^{-6} – 5.0\cdot10^{-5}$ m^2/s (Sharples et al., 2001) and $K_z=0.44 – 1.72\cdot10^{-4}$ m^2/s (Rippeth et al., 2009). Taking the typical length scale of the thermocline to be 10-20 m, this would lead to a typical time-scale in the order of 50 days to 1 year.

In summary, there are several hydrodynamic timescales: in general, there exist an advective time-scale of the order of 1 month related to the current system and a tidal time-scale of 0.5 (semi-diurnal) to 14 days (spring-neap tidal cycle). In winter, the vertical mixing time-scale is of the order of 10 days. In contrast, the vertical mixing time-scale in summer is roughly 50 days to 1 year due to the reduced vertical exchange across the pycnocline and therefore comparable or longer than the biannual onset and breakdown of stratification. Changes in the timing of the onset and breakdown of the thermocline in a changing climate (section 2.9) will therefore affect the residence time of dissolved methane in the lower layer in the stratified season. In the surface and bottom mixed layer, the time-scale of vertical exchange is comparable to that of the winter mixed layer. In summer, tidal mixing fronts separating vertical well-mixed region from stratified region introduce additional time-scales in the horizontal, e.g. an along-frontal time-scale of 80 days over a length of 500 km due to the frontal-jet and a cross-frontal exchange of 0.5 to 1 days due to cross-frontal circulation and in the order of 2-3 days due to eddy-induced diffusion. Comparing the hydrodynamic time-scales with the methane oxidation time-scale (next section) will provide an answer to the fate of the methane under the various hydrodynamics conditions discussed above.

3.2 Methane oxidation Time Scales

All studies investigating the propagation of methane in the area of the 22/4b blowout site consistently show that by far the largest fraction of methane released at site is dissolved below the thermocline (Leifer et al., 2015; Schneider von Deimling et al., 2015; Sommer et al., 2015). While this finding appears to contradict with enhanced vertical transport in areas of strong seepage (Leifer et al., 2009; Leifer et al., 2006), observations of Schneider von Deimling et al. (2015) clearly suggest that the vigorous gas flow in combination to strong horizontal currents foster the formation of vortex structures as well as separation

of the gas flow from the upwelling plume, and propose this mechanism to explain the formerly unexpected high fraction of methane from this vigorous plume across the mixed layer. Model simulations by Leifer et al. (2015) also clearly indicate that the observed low surface flux of methane cannot be explained without a mechanism enhancing methane dissolution at depth, and try simple model approximations for vortex formation and turbulence-enhanced gas transfer velocities at the bubble boundary. In any case, the different studies based on data gathered in between May and October (of different years) all confirm that more than 95% of the gas was trapped below the thermocline. Thus, the question what fraction of methane released at the well site 22/4b blowout reaches the atmosphere requires an understanding of the plume behavior during the non-stratified season as well as an evaluation of the fate of methane dissolved below the thermocline during the stratified season. This also holds true for most other known natural or anthropogenic seabed sources in the North Sea. Schneider von Deimling et al. (2011) showed that the dissolution of bubbles released from the gas seeps in the Tommeliten area resulted in a fraction of only 4% that directly reached the upper well-mixed waters above the thermocline. A similar fate can be assumed for gas from other seep locations in the North Sea, such as Gullfaks, Witch Ground and Fladen, all located in seasonally stratified waters (Hovland and Judd, 1988), and gas released from abandoned well sites (Vielstädte et al., 2015), a recently discovered phenomenon that might be present in wide areas of the North Sea.

The non-stratified period at the blowout extends from November till April (see Figure 10), and site 22/4b is apparently at a location with an early onset and late breakdown of seasonal stratification (Fig. 10, plots for April and November). The behavior of the gas and upwelling plume during this period remains speculative due to a lack of observational data, as all of the field studies at site 22/4b were executed during the stratified period, and is beyond the scope of this paper. However, it is noteworthy that locally, the blowout-induced upwelling can lead to a local early breakdown of stratification, potentially enhancing the period of time favoring gas transport to the upper water layers (Nauw et al., 2015). With water depths in most parts of the North Sea not exceeding 150 m, and piston velocities for air-sea exchange above the global average (Liss and Merlivat, 1986; Wanninkhof et al., 2009) due to high wind stress, the timescale for methane to be vented to the atmosphere will be in the order of days to a maximum of a few weeks as the timescale of vertical transport of methane in unstratified areas/periods is less than a day. This is in accordance to the consideration of hydrodynamic time scales in well mixed areas/seasons presented in chapter 3.1. Also, the enhanced mixing will result in rapid dilution of the water from the plume area. As will be reasoned below, it thus appears likely that the flux of dissolved methane to the surface and the subsequent release to the atmosphere is high during well-mixed stormy autumn and winter conditions, as the residence time is too short for methane oxidation in the water column (Figure 23)

Still, between April/May and October/November (Figure 10), the bulk of the gas released at depth dissolves in the water column below the thermocline, where its further transport is determined by the hydrodynamic setting reviewed in this paper. The time scale for cross-thermocline mixing will be longer than the 23 days due to the stronger stratification and small wind-stress compared to the situation in late autumn, i.e. in the order of months. Methane that is trapped under the summer thermocline may thus be transferred horizontally over long distances to shallower areas / stratification fronts and exchanged with the atmosphere elsewhere. As discussed above, transport across seasonal tidal mixing fronts is generally reduced, though complex mixing processes can occur (see section 3.1 and Hill et al., 2008).

During the residence time in the water column, methane can be converted to carbon dioxide by aerobic methane oxidation. To estimate the time scale for oxidation in this methane-rich, well-oxygenated setting, we compiled data reported in the literature for methane turnover rates in marine settings (Figure 23).

The data compiled from various settings, including estuaries, gas hydrate dominated areas, and coastal regions, show a general trend of decreasing methane lifetime with increasing methane concentration. This is supported by Elliott et al. (2011), who suggest an empirical log linear relation based on a compilation of existing data. Considerable scatter exist both within individual data sets as well as between different studies. The data gathered in hydrothermal systems (de Angelis et al., 1993; Kadko et al., 1990), where the release of methane is linked to the release of heat, shows a distinct shift towards lower turnover times, potentially a cause of accelerated methane oxidation at higher temperatures, or due the presence of particles favoring microbial growth. The colder open ocean and coastal data (all other studies referenced in the caption of Figure 23), which are more representative for the situation at the 22/4b blowout site, suggest specific turnover times in the order between a month and a year for the enhanced concentrations > 100 nmol even some km away from the blowout site, potentially even shorter in the crater area where extremely high concentrations (up to 400.000 nmol/l, i.e. 400 μM) have been encountered (Schneider von Deimling et al., 2015). To date, unfortunately, no direct measurements of methane oxidation rates within the water column at well site 22/4b or elsewhere in the Northern North Sea have been reported. However, some data at the site have been collected in summer 2012 (Steinle et al., 2013), and support the general inverse correlation of methane concentration and turnover time, with rapid oxidation rates only in the plume and at the thermocline (Lea Steinle, University of Basel, pers. communication). Schmale et al. (2013) recently demonstrated the ability of gas bubbles to transport methanotrophs from the sediment into the water column, which might be a process sustaining the microbial communities above the site. However, Schneider von Deimling et al., (2015) compiled data on the stable carbon isotopic signature of methane around site 22/4b, which does not unambiguously show any sign of non-neglible methane oxidation.

Considering the time scales of a month for horizontal transport (possibly into non-stratified regions of the North Sea) as well as for vertical mixing across the thermocline (section 3.1) and our best knowledge on methane oxidation turnover in the water column, it appears likely that even during the stratified season, most of the methane will be transferred to the atmosphere, though not dominantly in the immediate vicinity of well site 22/4b. The observation that most of the methane is dissolved below the thermocline thus will lead to considerable displacement and temporal shift of the methane emission, though the loss due to oxidation can be expected to be small.

Discussion and Summary

In this review we attempted to summarize the current knowledge about the processes involved in the redistribution of methane released at a seabed source. As part of the methane released at site 22/4b will be dissolved locally, it will be transported by the local currents and therefore its spreading will be strongly dependent on the hydrodynamics of the North Sea. The hydrodynamics of the North Sea are dominated by tidally driven, wind-driven and (seasonally variable) density driven currents, but also determined by currents forced in the North Atlantic Ocean. Due to summertime heating the northern part of the North Sea becomes stratified. In autumn, cooling adds to the buoyancy loss to the atmosphere; the stratification breaks down slowly until at a certain moment the mixing induced by tides, storms, internal wave breaking and inertial current shear mixes the entire water column. During the period of (re)-stratification, the water column is divided into two or more layers, which can and will move independently.

The tidal wave travels in the anti-clockwise direction through the North Sea and drives an average anti-clockwise circulation by non-linear interaction with topography through bottom friction. Wind forcing over the North Sea may strengthen this cyclonic circulation; however, it can also have the opposing effect and halt this circulation, or even turn it around into a clockwise rotating flow, depending on the wind speed and direction. Climate change or variability adds its part to the complexity of the circulation

in the North Sea. The North Atlantic Oscillation (NAO) causes variability in the wind stress and direction over the North Sea due to variations in the large scale pressure system over the North Atlantic. A positive (negative) NAO index is associated with stronger (weaker) than normal westerly winds. Under NAO+ situations the circulation in the North Sea strengthens and long-term mean currents at site 22/4b are stronger and directed eastward, whereas they weaken during NAO- conditions and are directed northeastward. Besides this, the NAO also influences the Sea Surface Temperature (SST) of the North Sea. High positive correlations were found between the SST at site 22/4b and the NAO index. Another source of variability on timescales from annual to interannual is brought about by the currents entering the northern part of the North Sea from the adjacent Atlantic Ocean. Especially, the Fair Isle Current (FIC), entering the North Sea between the Orkney and the Shetland Islands, may be significant as it passes (on average) site 22/4b and displays strong variability in terms of temperature and salinity. Seasonally varying stratification adds a density-driven component to the residual current structure, which locally at site 22/4b strengthens the residual current brought about by the FIC. When the seasonal front passes the location, strong local sub-surface cross-frontal jets will be generated. Modelling studies suggest that in the future warming climate SST will increase and Sea Surface Salinity will decrease, leading to a strengthening of the stratification and prolonged duration of the period of stratification (Ådlandsvik, 2008, Dye et al., 2013; Holt et al., 2010, Nakicenovic and Swart, 2000l Mathis and Pohlmann, 2014). Holt et al. (2014) discussed that the influence of climate change is slightly more subtle and could (under certain conditions) also lead to a reduction in strength and duration of the seasonal stratification. The transport of dissolved methane across the thermocline in the stratified period of the year is inhibited and therefore has implication for the horizontal dispersion of the methane and the period of biodegradation.

To determine the fate of methane, we need to consider both the variation in oxidation rates under different circumstances and the time-scales introduced by the hydrodynamics. Oxidation turnover times for areas representative for the situation at site 22/4b are in the order of one month for concentrations as high as the ones found there, but considerably longer once the plume gets diluted. During the non-stratified part of the season (November till March), mixing and ventilation to the atmosphere is rapid, and the gas released at site 22/4b is expected to be ventilated to the atmosphere almost instantaneously.

During the part of the year with a stratified water column, time-scales associated with the vertical mixing and oxidation in the vicinity of the plume are the same order of magnitude, but time-scales associated with the residual circulation, bubble momentum plume induced vertical mixing and along- and cross-frontal circulation upon passage of the tidal mixing front are much smaller. This leads to a complex interaction between the circulation/hydrography on the one hand and the oxidation of methane on the other.

Investigations during the winter period as well as during the time of the breakdown of stratification in autumn, including hydrographic, gas chemical, as well as microbiological measurements, would be needed to experimentally verify the conclusions drawn here and identify the most important processes involved in the degradation of methane. These processes need to be incorporated into an ecosystem model, such as ERSEM (Baretta et al., 1995) coupled to a hydrodynamic numerical model and an atmospheric model to establish the fate of methane that is released at the seafloor at site 22/4b (if the exact amount is known, Leifer and Judd, 2015). Using this model, one should be able to estimate the amount that will be released to the atmosphere, which can be compared with observations of the atmospheric methane concentrations (Gerilowski et al., 2015; Judd, 2015).

Acknowledgements

The authors would like to acknowledge the assistance of ExxonMobil International Ltd with the development of this publication. We also wish to thank the anonymous reviewers for their valuable comments and suggestions on the manuscript.

Bibliography

Ådlandsvik, B., 2008. Marine downscaling of a future climate scenario for the North Sea. Tellus A 60 (3), 451–458.

Andersson, L., Rydberg, L., 1993. Exchange of water and nutrients between the Skagerrak and the Kattegat. Estuarine, Coastal and Shelf Science 36 (2), 159 – 181.

Backhaus, J., 1985. A three-dimensional model for the simulation of shelf sea dynamics. Deutsche Hydrografische Zeitschrift 38, 165–187.

Backhaus, J. O., 1984. Estimates of the variability of low frequency currents and flushing-times of the North Sea.

Badin, G., Williams, R. G., Holt, J. T., Fernand, L. J., 2009. Are mesoscale eddies in shelf seas formed by baroclinic instability of tidal fronts? Journal of Geophysical Research: Oceans 114 (C10).

Baretta, J., Ebenhöh, W., Ruardij, P., 1995. The European Regional Seas Ecosystem Model, a complex marine ecosystem model. Netherlands Journal of Sea Research 33 (3), 233–246.

Beaugrand, G., 2004. The North Sea regime shift: Evidence, causes, mechanisms and consequences. Progress in Oceanography 60 (2-4), 245 – 262.

Becker, G., Dooley, H., 1995. The 1989/91 High Salinity Anomaly in the North Sea and adjacent areas. Ocean Challenge 6, 52–57.

Becker, G. A., Pauly, M., 1996. Sea surface temperature changes in the North Sea and their causes. ICES Journal of Marine Science: Journal du Conseil 53 (6), 887–898.

Berx, B., Hughes, S. L., 2009. Climatology of surface and near-bed temperature and salinity on the north-west European continental shelf for 1971-2000. Continental Shelf Research 29 (19), 2286 – 2292.

Blaas, M., Kerkhoven, D., de Swart, H. E., 2001. Large-scale circulation and flushing characteristics of the North Sea under various climate forcings. Climate Research 18 (1/2), 47–54.

Bolding, K., Burchard, H., Pohlmann, T., Stips, A., 2002. Turbulent mixing in the Northern North Sea: a numerical model study. Continental Shelf Research 22 (18-19), 2707 – 2724, physics of Estuaries and Coastal Seas, Volume II: Proceedings of the tenth biennial conference, Norfolk, Virginia, USA, 7-11 October 2000.

Bowers, D., Simpson, J., 1987. Mean position of tidal fronts in European-shelf seas. Continental Shelf Research 7 (1), 35 – 44.

Brettschneider, G., 1967. Anwendung des hydrodynamisch-numerischen Verfahrens zur Ermittlung der M2-Mitschwingungsgezeit der Nordsee. Tech. Rep. 7, Mitt. Inst. Meereskd. Univ. Hamburg, 65 pp.

Brown, J., Hill, A., Fernand, L., Horsburgh, K., 1999. Observations of a seasonal jet-like circulation at the central North Sea cold pool margin. Estuarine, Coastal and Shelf Science 48 (3), 343 – 355.

Burchard, H., Bolding, K., 2002. GETM, a general estuarine transport model. Tech. rep., European Commission, Ispra.

Burchard, H., Rippeth, T. P., 2009. Generation of bulk shear spikes in shallow stratified tidal seas. J. Phys. Oceanogr. 39 (4), 969–985.

Danielssen, D. S., Edler, L., Fonselius, S., Hernroth, L., Ostrowski, M., Svendsen, E., Talpsepp, L., 1997. Oceanographic variability in the Skagerrak and Northern Kattegat, May–June, 1990. ICES Journal of Marine Science: Journal du Conseil 54 (5), 753–773.

De Angelis, M., Lilley, M., Baross, J., 1993. Methane oxidation in deep-sea hydrothermal plumes of the Endeavour Segment of the Juan de Fuca Ridge. Deep Sea Research Part I: Oceanographic Research Papers 40 (6), 1169–1186.

de Haas, H., Greinert, J., Urban, P., van Gaever, P., 2012. Listen to the bubbles, see the bubbles, catch the bubbles: Methane seepage in the North Sea. In: 11th Dutch Earth Sciences Conference.

de Haas, H., Shipboard Scientific Crew, ., 2011. Cruise report RV Pelagia cruise 64PE340, North Sea Monitoring. Tech. rep., Royal Netherlands Institute for Sea Research.

Dickson, R. R., Meincke, J., Malmberg, S.-A., Lee, A. J., 1988. The "Great Salinity Anomaly" in the Northern North Atlantic 1968-1982. Progress in Oceanography 20 (2), 103 – 151.
Dooley, H., 1983. Seasonal Variability in the Position and Strength of the Fair Isle Current. In: Sündermann, J., Lenz, W. (Eds.), North Sea Dynamics. Springer Berlin Heidelberg, pp. 108–119.
Dooley, H., Furnes, G., 1981. Influence of the wind field on the transport in of the Northern North Sea. In: Saetre, R., Mork, M. (Eds.), The Norwegian Coastal Current. University of Bergen, pp. 57–71.
du Bois, P., Salomon, J., Gandon, R., Guéguéniat, P., 1995. A quantitative estimate of English Channel water fluxes into the North Sea from 1987 to 1992 based on radiotracer distribution. Journal of Marine Systems 6 (5-6), 457 – 481.
Dye, S., Hughes, S., Tinker, J., Berry, D., Holliday, N., Kent, E., Kennington, K., Inall, M., Smyth, T., Nolan, G., Lyons, K., Andres, O., Beszczynska-Möller, A., 2013. Impacts of climate change on temperature (air and sea). MCCIP Science Review, 1–12.
Egbert, G. D., Erofeeva, S. Y., Ray, R. D., 2010. Assimilation of altimetry data for nonlinear shallow-water tides: Quarter-diurnal tides of the Northwest European Shelf. Continental Shelf Research 30 (6), 668 – 679.
Eisma, D., Jansen, J., van Weering, T. C., et al., 1979. Sea-floor morphology and recent sediment movement in the North Sea. In: Acta Universitatis Upsaliensis. Symposia Universitatis Upsaliensis Annum Quingentesimum Celebrantis. Vol. 2.
Elliott, S., Maltrud, M., Reagan, M., Moridis, G., Cameron-Smith, P., 2011. Marine methane cycle simulations for the period of early global warming. Journal of Geophysical Research: Biogeosciences (2005–2012) 116 (G1).
Emery, W., Thomson, R., 1997. Data analysis methods in physical oceanography. Pergamon Press.
Gerilowski, J., Krings, T., Hartmann, J., Buchwitz, M., Sachs, T., Erzinger, J., Burrows, J. P., Bovensmann, H., 2015. Methane remote sensing constraints on direct sea-air flux flor the 22/4b North Sea massive blowout bubble plume. Journal of Marine and Petroleum Geology this issue.
Graham, C., 1985. Forties sheet 57°n - 00° including part of cod 57°n - 02°e. Tech. rep., British Geological Survey 1:250,000 Series, SeaBed Sediments.
Gupta, S., 2010. Practical density measurement and hydrometry. CRC Press.
Hill, A. E., Brown, J., Fernand, L., Holt, J., Horsburgh, K. J., Proctor, R., Raine, R., Turrell, W. R., 2008. Thermohaline circulation of shallow tidal seas. Geophysical Research Letters 35 (11).
Hill, A. E., James, I. D., Linden, P. F., Matthews, J. P., Prandle, D., Simpson, J. H., Gmitrowicz, E. M., Smeed, D. A., Lwiza, K. M. M., Durazo, R., Fox, A. D., Bowers, D. G., Weydert, M., 1993. Dynamics of tidal mixing fronts in the North Sea [and discussion]. Philosophical Transactions of the Royal Society of London. Series A: Physical and Engineering Sciences 343 (1669), 431–446.
Hoitink, A. J. F., Hoekstra, P., van Maren, D. S., Oct. 2003. Flow asymmetry associated with astronomical tides: Implications for the residual transport of sediment. J. Geophys. Res. 108 (C10), 3315–.
Holt, J., Hughes, S., Hopkins, J., Wakelin, S. L., Holliday, N. P., Dye, S., González-Pola, C., Hjøllo, S. S., Mork, K. A., Nolan, G., Proctor, R., Read, J., Shammon, T., Sherwin, T., Smyth, T., Tattersall, G., Ward, B., Wiltshire, K. H., 2012. Multi-decadal variability and trends in the temperature of the northwest European continental shelf: A model-data synthesis. Progress in Oceanography 106 (0), 96 – 117.
Holt, J., Proctor, R., 2008. The seasonal circulation and volume transport on the northwest European continental shelf: A fine-resolution model study. Journal of Geophysical Research: Oceans 113 (C6).
Holt, J., Schrum, C., Cannaby, H., Daewel, U., Allen, I., Artioli, Y., Bopp, L., Butenschon, M., Fach, B. A., Harle, J., Pushpadas, D., Salihoglu, B., Wakelin, S., 2014. Physical processes mediating climate change impacts on regional sea ecosystems. Biogeosciences Discussions 11 (2), 1909–1975.
Holt, J., Umlauf, L., 2008. Modelling the tidal mixing fronts and seasonal stratification of the Northwest European continental shelf. Continental Shelf Research 28 (7), 887 – 903.

Holt, J., Wakelin, S., Lowe, J., Tinker, J., 2010. The potential impacts of climate change on the hydrography of the northwest European continental shelf. Progress in Oceanography 86, 361 – 379.
Hordoir, R., Meier, H., 2010. Freshwater fluxes in the Baltic Sea: A model study. Journal of Geophysical Research: Oceans 115 (C8), 1978–2012.
Hovland, M., Judd, A. G., 1988. Seabed pockmarks and seepages: impact on geology, biology and the marine environment.
Howarth, M., Simpson, J., Sündermann, J., van Haren, H., 2002. Processes of Vertical Exchange in Shelf Seas (PROVESS). Journal of Sea Research 47 (3-4), 199 – 208.
Hulme, M., Jenkins, G., Turnpenny, J., Mitchell, T., Jones, R., Lowe, J., Murphy, J., Hassell, D., Boorman, P., McDonald, R., Hill, S., 2002. Climate Change Scenarios for the United Kingdom: The UKCIP02 Scientific Report. Tech. rep., Tyndall Centre for Climate Change Research, School of Environmental Sciences, University of East Anglia, Norwich UK.
Hurrell, J., Aug. 1995. Decadal trends in the North Atlantic Oscillation: regional temperatures and precipitation. Science 269 (5224), 676–679.
Håvelsrud, O., Haverkamp, T., Kristensen, T., Jakobsen, K., Rike, A., 2012. Metagenomic and geochemical characterization of pockmarked sediments overlaying the Troll petroleum reservoir in the North Sea. BMC Microbiology 12, 203.
ICES, 1983. Flushing times of the North Sea. Cooperative Research Report No. 123. Tech. rep., ICES.
ICES, 2005. The Annual ICES Ocean Climate Status Summary 2004/2005. Tech. rep., ICES Cooperative Research Report, No. 275. 37 pp.
ICES 2007b, 2007. North Sea ICES2007b conditions – 1st quarter 2007. Tech. Rep. ICES/EuroGOOS North Sea Pilot Project–NORSEPP, ICES/EuroGOOS Planning Group for NORSEPP (PGNSP), iCES/EuroGOOS Planning Group for NORSEPP (PGNSP).
Janssen, F., Schrum, C., Backhaus, J., 1999. A climatological data set of temperature and salinity for the Baltic Sea and the North Sea. Deutsche Hydrografische Zeitschrift 51, 5–245.
Jones, R. D., Amador, J. A., 1993. Methane and carbon monoxide production, oxidation, and turnover times in the Caribbean Sea as influenced by the Orinoco River. Journal of Geophysical Research: Oceans (1978–2012) 98 (C2), 2353–2359.
Judd, A., 2015. The significance of the 22/4b blow-out site methane emissions in the context of the North Sea. Journal of Marine and Petroleum Geology (this issue).
Judd, A. G., 2004. Natural seabed gas seeps as sources of atmospheric methane. Environmental Geology 46, 988–996.
Kadko, D., Rosenberg, N., Lupton, J., Collier, R., Lilley, M., 1990. Chemical reaction rates and entrainment within the endeavour ridge hydrothermal plume. Earth and Planetary Science Letters 99 (4), 315–335.
Kauker, F., von Storch, H., Dec. 2000. Statistics of synoptic circulation weather in the North Sea as derived from a multiannual OGCM Simulation. J. Phys. Oceanogr. 30 (12), 3039–3049.
Kirby, R. R., Beaugrand, G., 2009. Trophic amplification of climate warming. Proceedings of the Royal Society B: Biological Sciences 276 (1676), 4095–4103.
Klein, H., Lange, W., Mittelstaedt, E., 1994. Tidal and residual currents in the northern North Sea: Observations. Deutsche Hydrografische Zeitschrift 46 (1), 5–27.
Knight, P., Howarth, M., Rippeth, T., 2002. Inertial currents in the northern North Sea. Journal of Sea Research 47 (3-4), 269 – 284.
Le Boyer, A., Cambon, G., Daniault, N., Herbette, S., Le Cann, B., Marie, L., Morin, P., 2009. Observations of the Ushant tidal front in September 2007. Continental Shelf Research 29 (8), 1026–1037.
Leifer, I., Jeuthe, H., Gjøsund, S., Johansen, V., 2009. Engineered and natural marine seep, bubble-driven buoyancy flows. J. Phys. Oceanography 39, 3071–3090.

Leifer, I., Judd, A., 2015. The UK22/4b blowout 20 years on: Investigations of continuing methane emissions from sub-seabed to the atmosphere in a North Sea context. Journal of Marine and Petroleum Geology (this issue).
Leifer, I., Luyendyk, B., Boles, J., Clark, J., 2006. Natural marine seepage blowout: Contribution to atmospheric methane. Global Biogeochemical Cycles 20.
Leifer, I., Solomon, E., Coffin, R., Rehder, G., Linke, P., 2015. The fate of bubbles in a large, intense bubble plume for stratified and unstratified water: Numerical simulations of 22/4b expedition field data. Journal of Marine and Petroleum Geology (this issue).
Lenhart, H.-j., Pohlmann, T., 1997. The ICES-boxes approach in relation to results of a North Sea circulation model. Tellus A 49 (1), 139–160.
Linke, P., Schmidt, M., cruise participants, C., 2010. RV Celtic Explorer Fahrtbericht / Cruise Report CE0913 Fluid and gas seepage in the North Sea. Tech. rep., IFM-GEOMAR.
Liss, P., Merlivat, L., 1986. Air-sea gas exchange rates: Introduction and synthesis. In: Buat-Ménard, P. (Ed.), The Role of Air-Sea Exchange in Geochemical Cycling. Vol. 185 of NATO ASI Series. Springer Netherlands, pp. 113–127.
Luff, R., Pohlmann, T., 1995. Calculation of water exchange times in the ices-boxes with an Eulerian dispersion model using a half-life time approach. Deutsche Hydrografische Zeitschrift 47 (4), 287–299.
Luyten, P., Carniel, S., Umgiesser, G., 2002. Validation of turbulence closure parameterisations for stably stratified flows using the PROVESS turbulence measurements in the North Sea. Journal of Sea Research 47 (3-4), 239 – 267.
Lwiza, K., Bowers, D., Simpson, J., 1991. Residual and tidal flow at a tidal mixing front in the North Sea. Continental Shelf Research 11 (11), 1379 – 1395.
Maas, L., van Haren, J., 1987. Observations on the vertical structure of tidal and inertial currents in the central North Sea. Journal of Marine Research 45 (2), 293–318.
MacKinnon, J. A., Gregg, M. C., 2005. Near-inertial waves on the New England Shelf: The role of evolving stratification, turbulent dissipation, and bottom drag. J. Phys. Oceanogr. 35 (12), 2408–2424.
Mathis, M. & Pohlmann, J., 2014. Projection of physical conditions in the North Sea for the 21st century. Clim. Res. 61 (1), 1-17.
Matthews, J., Fox, A., Prandle, D., 1993. Radar observation of an along-front jet and transverse flow convergence associated with a North Sea front. Continental Shelf Research 13 (1), 109 – 130.
McGinnis, D. F., Greinert, J., Artemov, Y., Beaubien, S. E., Wüest, A., Sep. 2006. Fate of rising methane bubbles in stratified waters: How much methane reaches the atmosphere? J. Geophys. Res. 111 (C9), C09007.
Meyer, E. M., Pohlmann, T., Weisse, R., 2011. Thermodynamic variability and change in the North Sea (1948-2007) derived from a multidecadal hindcast. Journal of Marine Systems 86 (3-4), 35 – 44.
Mork, K. A., Blindheim, J., 2000. Variations in the Atlantic inflow to the Nordic Seas, 1955-1996. Deep Sea Research Part I: Oceanographic Research Papers 47 (6), 1035 – 1057.
Nakicenovic, N., Swart, R., 2000. Special report on emission scenarios. A special report of working group III of the Intergovernmental Panel on Climate Change. Tech. rep., Cambridge University Press.
Nauw, J., Linke, P., Leifer, I., 2015. Bubble momentum plume as a mechanism for an early breakdown of the seasonal stratification in the northern North Sea. Journal of Marine and Petroleum Geology (this issue).
O'dea, E., Arnold, A., Edwards, K., Furner, R., Hyder, P., Martin, M., Siddorn, J., Storkey, D., While, J., Holt, J., Liu, H., 2012. An operational ocean forecast system incorporating NEMO and SST data assimilation for the tidally driven European North-West shelf. Journal of Operational Oceanography 5 (1), 3–17.
O'Sullivan, T. D., Smith, N. O., 1970. Solubility and partial molar volume of nitrogen and methane in water and in aqueous sodium chloride from 50 to 125. deg. and 100 to 600 atm. The Journal of Physical Chemistry 74 (7), 1460–1466.

Otto, L., Zimmerman, J., Furnes, G., Mork, M., Saetre, R., Becker, G., 1990. Review of the physical oceanography of the North Sea. Netherlands Journal of Sea Research 26 (2-4), 161 – 238.
Pingree, R., 2005. North Atlantic and North Sea Climate Change: curl up, shut down, NAO and Ocean Colour. Journal of the Marine Biological Association of the United Kingdom 85 (06), 1301–1315.
Pingree, R. D., 11 1978. Cyclonic eddies and cross-frontal mixing. Journal of the Marine Biological Association of the United Kingdom 58, 955–963.
Pingree, R. D., Griffiths, D. K., 1978. Tidal fronts on the shelf seas around the British Isles. Journal of Geophysical Research: Oceans 83 (C9), 4615–4622.
Plag, H.-P., Tsimplis, M., 1999. Temporal variability of the seasonal sea-level cycle in the North Sea and Baltic Sea in relation to climate variability. Global and Planetary Change 20 (2-3), 173 – 203.
Pohlmann, T., 1996. Simulating the heat storage in the North Sea with a three-dimensional circulation model. Continental Shelf Research 16 (2), 195 – 213.
Prandle, D., 1984. A modelling study of the mixing of ^{137}Cs in the seas of the European continental shelf. Philosophical Transactions of the Royal Society of London. Series A, Mathematical and Physical Sciences 310 (1513), 407–436.
Pugh, D. T., 1987. Tides, Surges and Mean Sea-Level. John Wiley & Sons.
Rehder, G., Keir, R. S., Suess, E., Pohlmann, T., 1998. The multiple sources and patterns of methane in North Sea waters. Aquatic Geochemistry 4, 403–427.
Rehder, G., Keir, R. S., Suess, E., Rhein, M., 1999. Methane in the northern Atlantic controlled by microbial oxidation and atmospheric history. Geophys. Res. Lett. 26 (5), 587–590.
Reid, P., Edwards, M., 2001. Long-term changes in the pelagos, benthos and fisheries of the North Sea. Senckenb. Marit. 31, 107–115.
Reid, P. C., de Fatima Borges, M., Svendsen, E., 2001. A regime shift in the North Sea circa 1988 linked to changes in the North Sea horse mackerel fishery. Fisheries Research 50 (1-2), 163 – 171.
Reid, P. C., Edwards, M., Beaugrand, G., Skogen, M., Stevens, D., 2003. Periodic changes in the zooplankton of the North Sea during the twentieth century linked to oceanic inflow. Fisheries Oceanography 12 (4-5), 260–269.
Ridderinkhof, H., Zimmerman, J. T. F., 1992. Chaotic stirring in a tidal system. Science 258 (5085), 1107–1111.
Rippeth, T. P., 2005. Mixing in seasonally stratified shelf seas: a shifting paradigm. Philosophical Transactions of the Royal Society A: Mathematical, Physical and Engineering Sciences 363 (1837), 2837–2854.
Rippeth, T. P., Palmer, M. R., Simpson, J. H., Fisher, N. R., Sharples, J., 2005. Thermocline mixing in summer stratified continental shelf seas. Geophysical Research Letters 32 (5).
Rippeth, T. P., Wiles, P., Palmer, M. R., Sharples, J., Tweddle, J., 2009. The diapcynal nutrient flux and shear-induced diapcynal mixing in the seasonally stratified western Irish Sea. Continental Shelf Research 29 (13), 1580 – 1587.
Rydberg, L., Haamer, J., Liungman, O., 1996. Fluxes of water and nutrients within and into the Skagerrak. Journal of Sea Research 35 (1-3), 23 – 38.
Schmale, O., Leifer, I., Schneider von Deimling, J., Stolle, C., Kiesslich, K., Krause, S., Frahm, A., Treude, T., 2013. Bubble shuttle: A newly discovered transport mechanism, which transfers microorganisms from the sediment into the water column.
Schmid, M., Lorke, A., Dinkel, C., Tanyileke, G., Wüest, A., 2004. Double-diffusive convection in Lake Nyos, Cameroon. Deep Sea Research Part I: Oceanographic Research Papers 51 (8), 1097–1111.
Schneider von Deimling, J., Linke, P., Schmidt, M., G., R., 2015. A mega methane gas plume with spiral vortex motion – insights about the abandoned Blowout site in the North Sea since 2005. Journal of Marine and Petroleum Geology (this issue).

Schneider von Deimling, J., Rehder, G., Greinert, J., McGinnnis, D., Boetius, A., Linke, P., 2011. Quantification of seep-related methane gas emissions at Tommeliten, North Sea. Continental Shelf Research 31 (7-8), 867 – 878.
Schroot, B. M., Klaver, G. T., Schüttenhelm, R. T., 2005. Surface and subsurface expressions of gas seepage to the seabed examples from the Southern North Sea. Marine and Petroleum Geology 22 (4), 499 – 515.
Scranton, M. I., Brewer, P. G., 1978. Consumption of dissolved methane in the deep ocean. Limnol. Oceanogr 23 (6), 1207–1213.
Sharples, J., Moore, M. C., Rippeth, T. P., Holligan, P. M., Hydes, D. J., Fisher, N. R., Simpson, J. H., 2001. Phytoplankton distribution and survival in the thermocline. Limnology and Oceanography 46 (3), 486–496.
Sharples, J., Ross, O. N., Scott, B. E., Greenstreet, S. P., Fraser, H., 2006. Inter-annual variability in the timing of stratification and the spring bloom in the North-western North Sea. Continental Shelf Research 26 (6), 733 – 751.
Siegismund, F., 2001. Long-term changes in the flushing times of the ICES-boxes. Senckenbergiana maritima 31 (2), 151–167.
Simpson, J. H., 1998. Tidal processes in shelf seas. The sea 10, 113–150.
Simpson, J. H., Crisp, D. J., Hearn, C., Sep. 1981. The shelf-sea fronts: Implications of their existence and behaviour [and discussion]. Philosophical Transactions of the Royal Society of London. Series A, Mathematical and Physical Sciences 302 (1472), 531–546.
Simpson, J. H., Pingree, R. D., 1978. Shallow sea fronts produced by tidal stirring. In: Bowman, M., Esaias, W. (Eds.), Oceanic Fronts in Coastal Processes. Springer Berlin Heidelberg, pp. 29–42.
Simpson, J. H., Sharples, J., 2012. Introduction to the physical and biological oceanography of shelf seas. Cambridge University Press.
Skogen, M. D., Svendsen, E., Berntsen, J., Aksnes, D., Ulvestad, K. B., 1995. Modelling the primary production in the North Sea using a coupled three-dimensional physical-chemical-biological ocean model. Estuarine, Coastal and Shelf Science 41 (5), 545 – 565.
Skogen, M. D., Svendsen, E., Ostrowski, M., 1997. Quantifying volume transports during SKAGEX with the Norwegian Ecological Model system. Continental Shelf Research 17 (15), 1817 – 1837.
Sündermann, J., Pohlmann, T., 2011. A brief analysis of North Sea physics. Oceanologia 53(3), 663–689.
Sommer, S., Schmidt, M., Linke, P., 2015. Continuous inline tracking of dissolved methane plume at a blow out site in the North Sea UK – water column stratification impedes immediate methane release into the atmosphere. Journal of Marine and Petroleum Geology (this issue).
Souza, A., Simpson, J., 1996. The modification of tidal ellipses by stratification in the Rhine ROFI. Continental Shelf Research 16 (8), 997 – 1007.
Steinle, L. I., Wilfert, P., Schmidt, M., Bryant, L., Haeckel, M., Lehmann, M. F., Linke, P., Sommer, S., Treude, T., Niemann, H., 2013. News from the "blowout", a man-made methane pockmark in the North Sea: chemosynthetic communities and microbial methane oxidation. In: EGU General Assembly Conference Abstracts. Vol. 15. p. 8017.
Sündermann, J., Becker, G., Damm, P., Eynde, D., Frohse, A., Laane, R., Leussen, W., Pohlmann, T., Raaphorst, W., Radach, G., Schultz, H., Visser, M., 1996. Decadal variability on the Northwest European Shelf. Deutsche Hydrografische Zeitschrift 48 (3-4), 365–400.
Svendsen, E., S, R., Mork, M., 1991. Features of the northern North Sea circulation. Continental Shelf Research 11 (5), 493 – 508.
Thomann, R. V., Mueller, J. A., 1987. Principles of Surface Water Quality Modeling and Control. Inc., New York.
Turrell, W., Henderson, E., 1990. Transport events within the Fair Isle current during the Autumn Circulation Experiment (ACE). Estuarine, Coastal and Shelf Science 31 (1), 25 – 44.

Turrell, W., Henderson, E., Slesser, G., 1990. Residual transport within the Fair Isle Current observed during the Autumn Circulation Experiment (ACE). Continental Shelf Research 10 (6), 521 – 543.
Turrell, W., Henderson, E., Slesser, G., Payne, R., Adams, R., 1992. Seasonal changes in the circulation of the northern North Sea. Continental Shelf Research 12 (2-3), 257 – 286.
Turrell, W. R., Slesser, G., Payne, R., Adams, R. D., Gillibrand, P. A., 1996. Hydrography of the East Shetland Basin in relation to decadal North Sea variability. ICES Journal of Marine Science: Journal du Conseil 53 (6), 899–916.
Valentine, D. L., Blanton, D. C., Reeburgh, W. S., Kastner, M., 2001. Water column methane oxidation adjacent to an area of active hydrate dissociation, Eel river Basin. Geochim. Cosmochim. Acta 65, 2633 - 2640
van Aken, H. M., van Heijst, G. J. F., Maas, L. R. M., 1987. Observations of fronts in the North Sea. Journal of Marine Research 45 (3), 579–600.
van den Hurk, B., Klein Tank, A., Lenderink, G., van Ulden, A., van Oldenborgh, G., Katsman, C., van den Brink, H., Keller, F., Bessembinder, J., Burgers, G., Komen, G., Hazeleger, W., Drijfhout, S., 2006. KNMI Climate Change Scenarios 2006 for the Netherlands. KNMI Scientific Report WR 2006-01.
van Haren, H., 2000. Properties of vertical current shear across stratification in the North Sea. Journal of Marine Research 58 (3), 465–491.
van Haren, H., Maas, L., Zimmerman, J. T. F., Ridderinkhof, H., Malschaert, H., 1999. Strong inertial currents and marginal internal wave stability in the central North Sea. Geophysical Research Letters 26 (19), 2993–2996.
Vielstädte, L., Karstens, J., Haeckel, M., Schmidt, M., Linke, P., Reimann, S., Liebetrau, V., McGinnis, D., Wallmann, K., 2015. Quantification of methane emissions at abandoned gas wells in the central North Sea. Journal of Marine and Petroleum Geology (this issue).
Wanninkhof, R., Asher, W. E., Ho, D. T., Sweeney, C., McGillis, W. R., 2009. Advances in quantifying air-sea gas exchange and environmental forcing. Annual Review of Marine Science 1 (1), 213–244.
Ward, B., Kilpatrick, K., Novelli, P., Scranton, M., 1987. Methane oxidation and methane fluxes in the ocean surface layer and deep anoxic waters. Nature 327 (6119), 226–229.
Ward, B., Kilpatrick, K., Wopat, A., Minnich, E., Lidstrom, M., 1989. Methane oxidation in Saanich Inlet during summer stratification. Continental Shelf Research 9 (1), 65–75.
Weijerman, M., Lindeboom, H., Zuur, A. F., 2005. Regime shifts in marine ecosystems of the North Sea and Wadden Sea. Marine Ecology Progress Series 298, 21–39.
Winther, N. G., Evensen, G., 2006. A hybrid coordinate ocean model for shelf sea simulation. Ocean Modelling 13 (3â€“4), 221 – 237.
Working group I, 2013. IPCC Fifth Assessment Report Climate Change 2013: The Physical Science Basis. Tech. rep., IPCC.
Zimmerman, J., 1986. The tidal whirlpool: a review of horizontal dispersion by tidal and residual currents. Netherlands Journal of Sea Research 20 (2), 133–154.

Figures

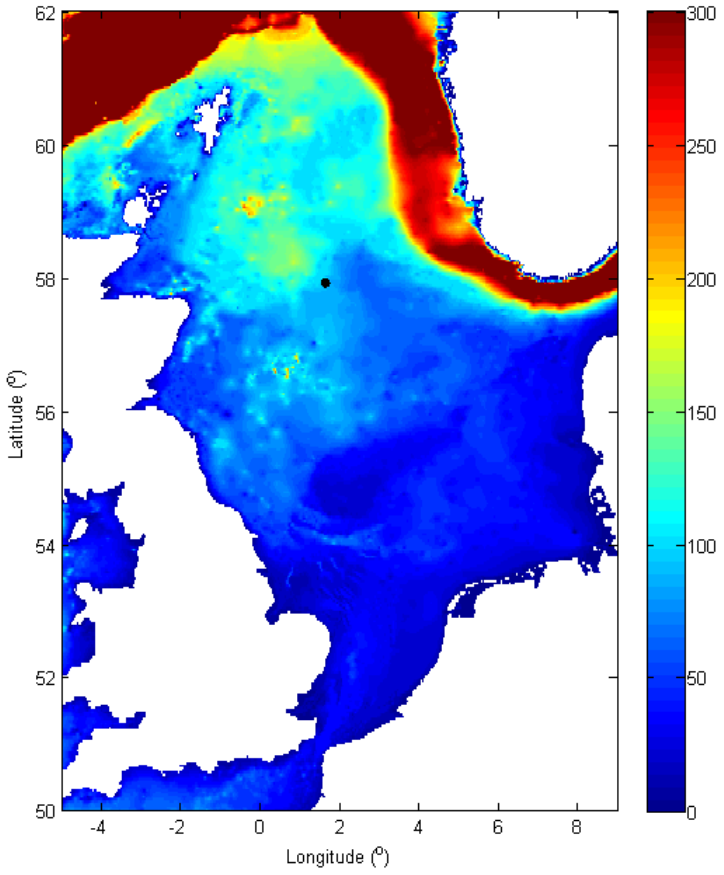

Figure 1: Bathymetry (m) of the European Shelf between 0 and 300 m from Gebco bathymetry at 1/30° resolution. The black dot indicates the location of site 22/4b.

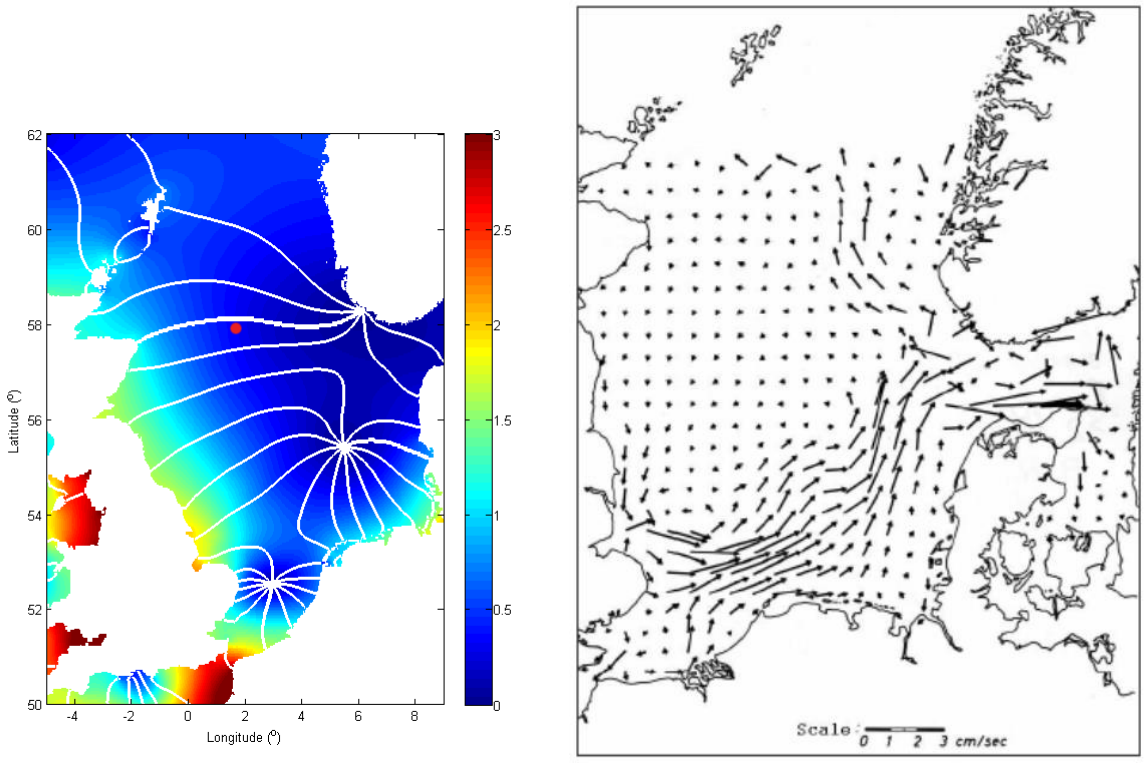

Figure 2: Left: tides in the North Sea as derived from OSU tidal model (Egbert et al., 2010). White lines are co-phase lines of the M_2 tide. Colors indicate the mean tidal amplitude. The red dot indicates the location of site 22/4b. Right: residual currents of the M_2-tide from (Brettschneider, 1967), figure reprinted from Figure 9 on page 672 of Sündermann and Pohlmann (2011).

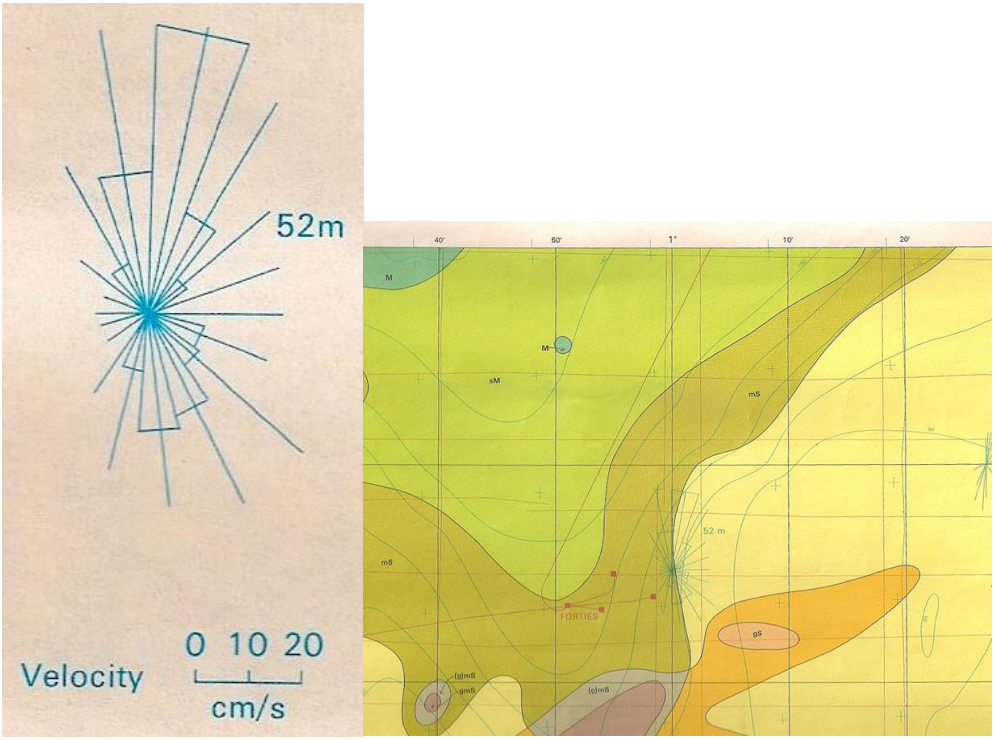

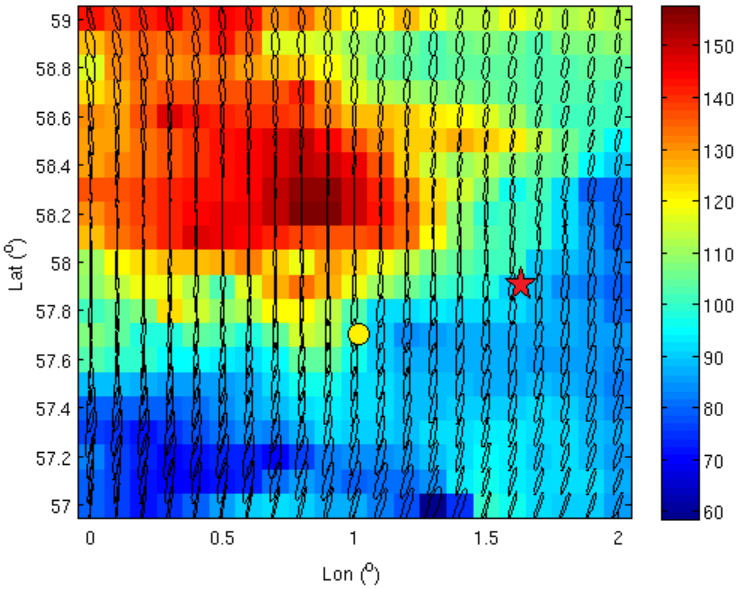

Figure 3: Top: tidal current measurements at the forties site at 53 m depth. Bottom: bathymetry (m) between 0 and 2 degrees East and 57 and 59 degrees North and on top of that the tidal ellipses of the M2 tidal component derived from the model by Egbert et al. (2010). The yellow circle indicates the location of the forties site and the red star the location of site 22/4b.

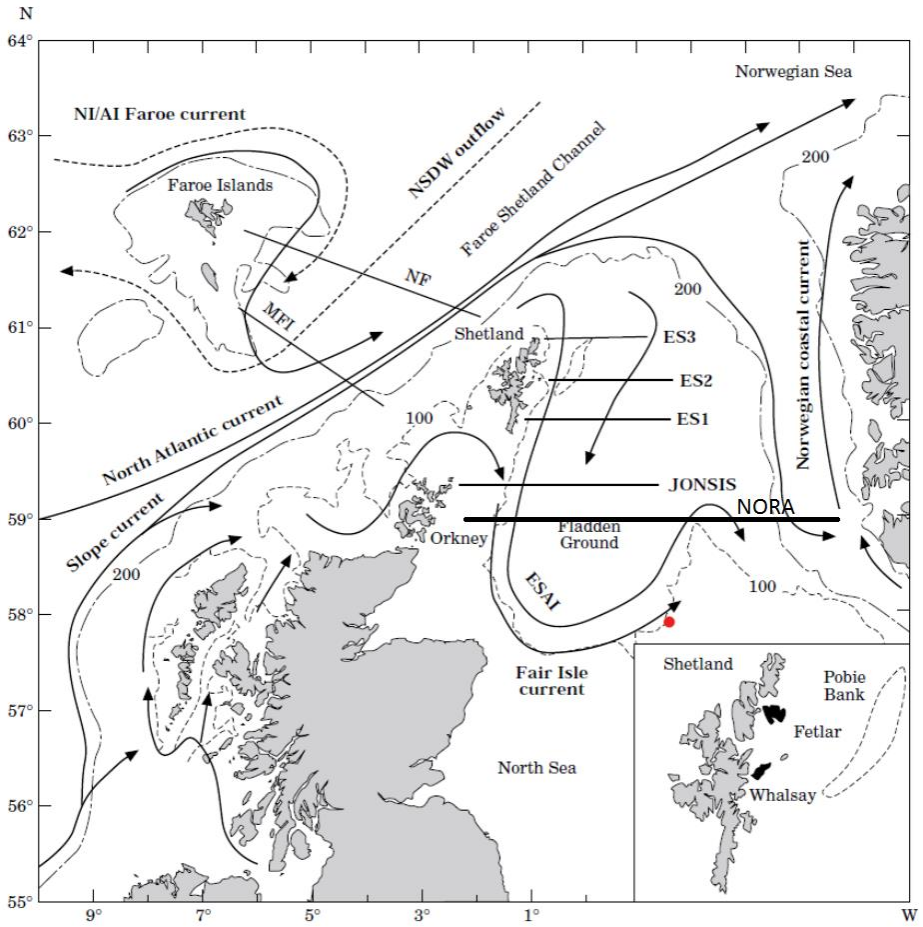

Figure 4: Map showing the key features of the topography of the North Sea and the adjacent oceanic areas in relation to the proposed circulation and the location of the standard hydrographic sections. Solid arrows represent surface circulation and broken arrows sub-surface. NF – Nolso-Flugga standard hydrographic section; MFI – Munken – Fair Isle section; ES1,2,3 – East Shetland sections; JONSIS – JOint North Sea Information Section; NORA – NordRand section; ESAI – East Scotland Atlantic Inflow; NI/AI – North of Iceland/Arctic intermediate water; NSDW – Norwegian Sea Deep Water. Insert shows details and local names of features east of Scotland. The red dot marks the approximate location of site 22/4b, slightly modified from Figure 1 on page 900 of Turrell et al. (1996).

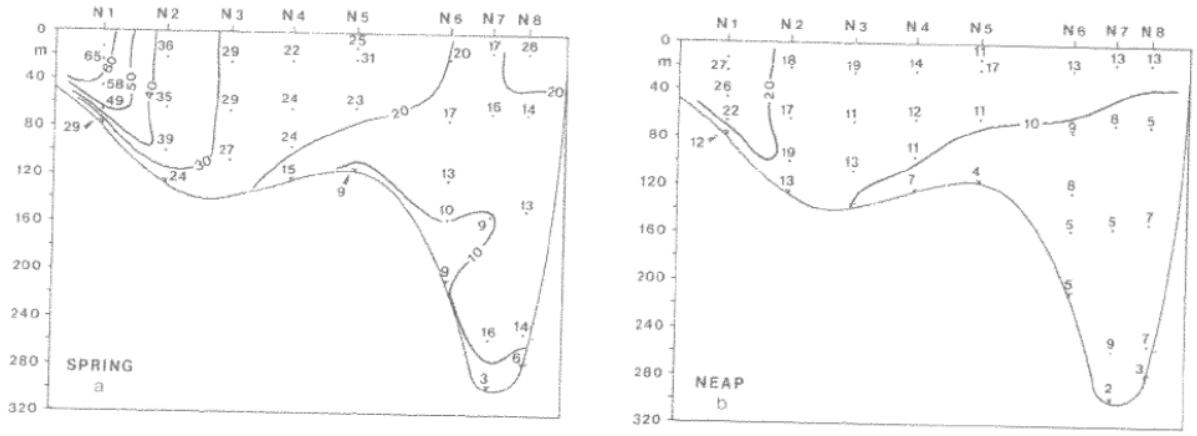

Figure 5: Mean maximum spring (a) and neap (b) speeds in cm/s in the NORA section indicated in Figure 4. Reprinted from Figure 6 on page 15 in Klein et al. (1994).

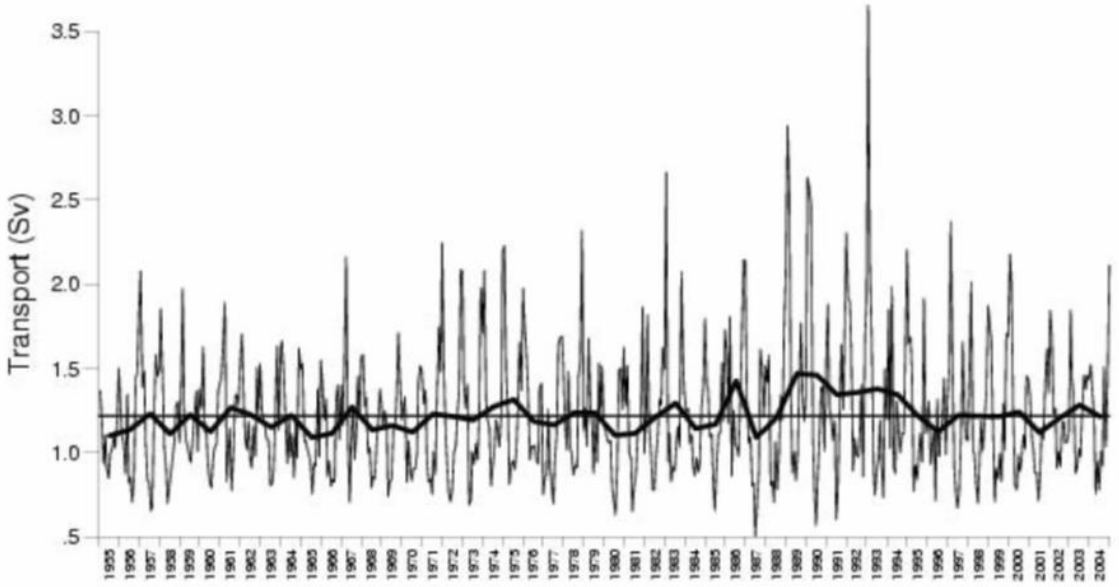

Figure 6: Time-series (1955-2004) of modeled annual mean (bold) and monthly mean volume transport of Atlantic water into the northern and central North Sea southward between the Orkney Islands and Utsira Norway. 1 Sv =10^6 m^3/s (anon, 2005), reprinted from Figure 34 on page 27 of ICES (2005).

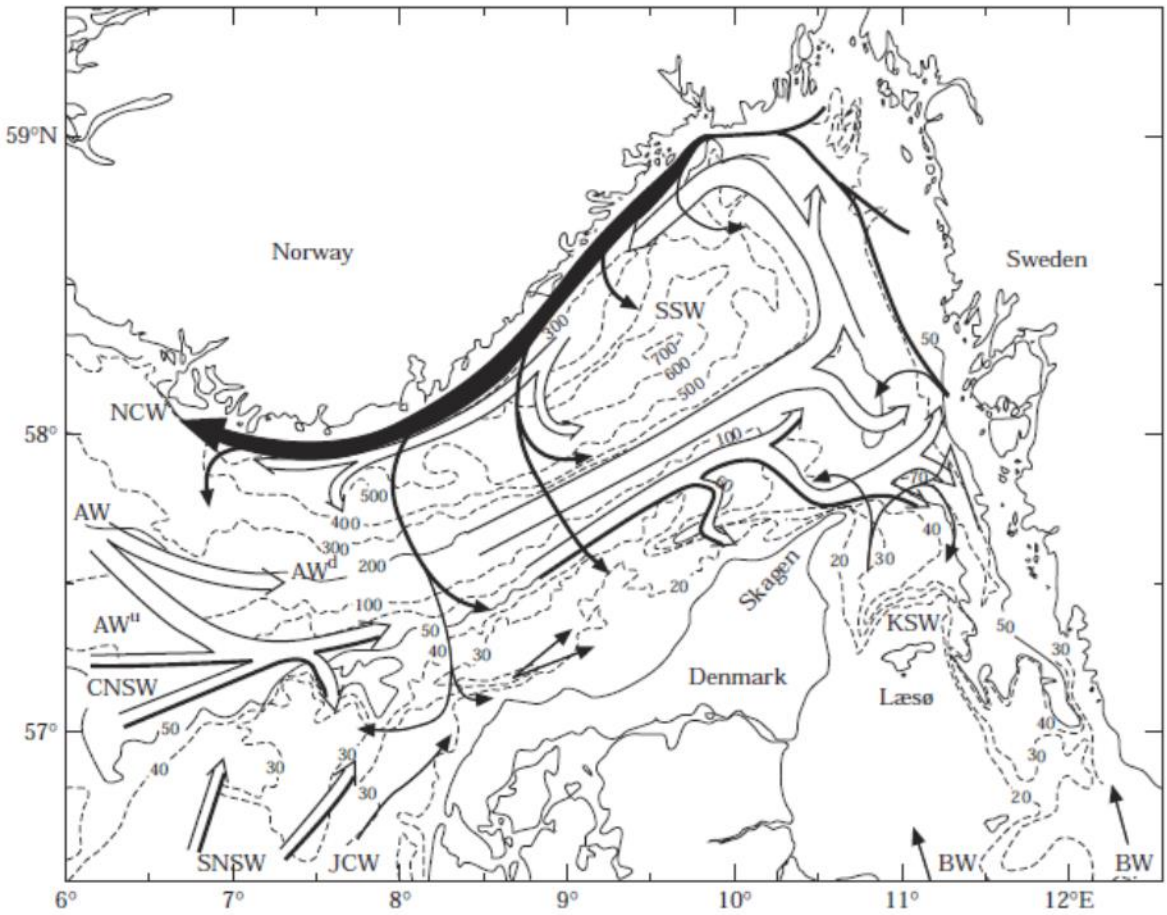

Figure 7: Schematics of the general circulation of the relevant water masses in the Skagerrak and adjacent areas. Open and filled arrows indicate subsurface and surface water, respectively. AW= Atlantic Water, AW^{u}= Atlantic water upper (shallow), AW^{d}=Atlantic water deep (deep), BW=Baltic Water CNSW=Central North Sea Water, JCW=Jutland Coastal Water, KSW=Kattegat Surface Water, NCW=Norwegian Coastal Water, SNSW=Southern North Sea Water, SSW=Skagerrak Surface Water, reprinted from Figure 1 on page 655 of Danielssen et al. (1997).

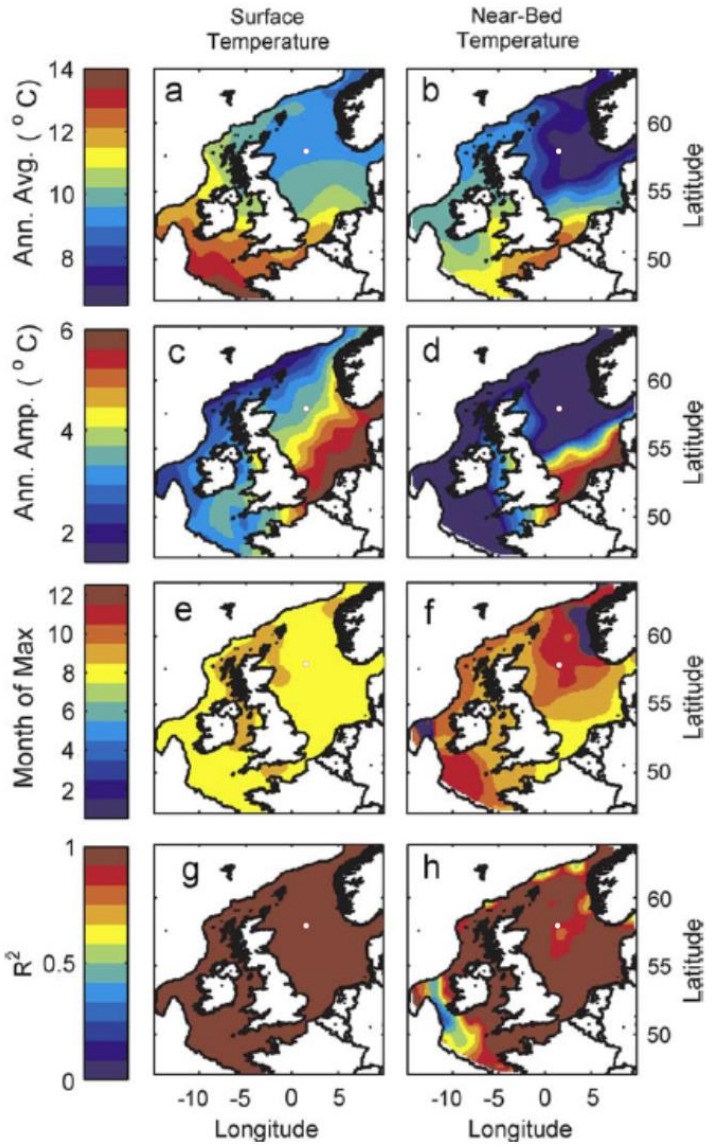

Figure 8: Left- surface layer, right near bed layer: (a,b) annual mean temperature (°C), (c,d) annual seasonal cycle amplitude (°C), (e.f) phase (expressed as month of maximum), and (g,h) R^2 of the harmonic analysis method of least squares (HAMELS, Emery and Thomson, 1997) analysis for the period 1971-2000. The white dot marks the approximate location of site 22/4b, slightly modified from Figure 2 on page of 2289 of Berx and Hughes (2009).

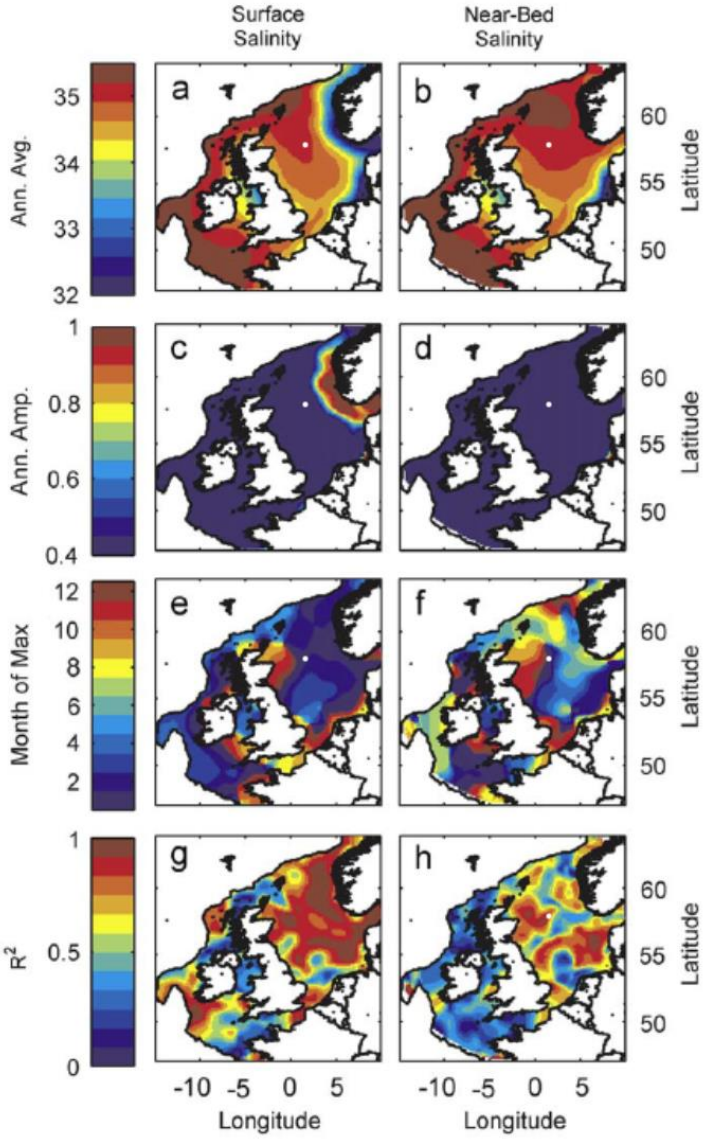

Figure 9: Left- surface layer, right near bed layer: (a,b) annual mean salinity, (c,d) annual seasonal cycle amplitude, (e.f) phase (expressed as month of maximum), and (g,h) R^2 of the harmonic analysis method of least squares (HAMELS, Emery and Thomson, 1997) analysis for the period 1971-2000. The white dot marks the approximate location of site 22/4b, slightly modified from Figure 3 on page of 2289 of Berx and Hughes (2009).

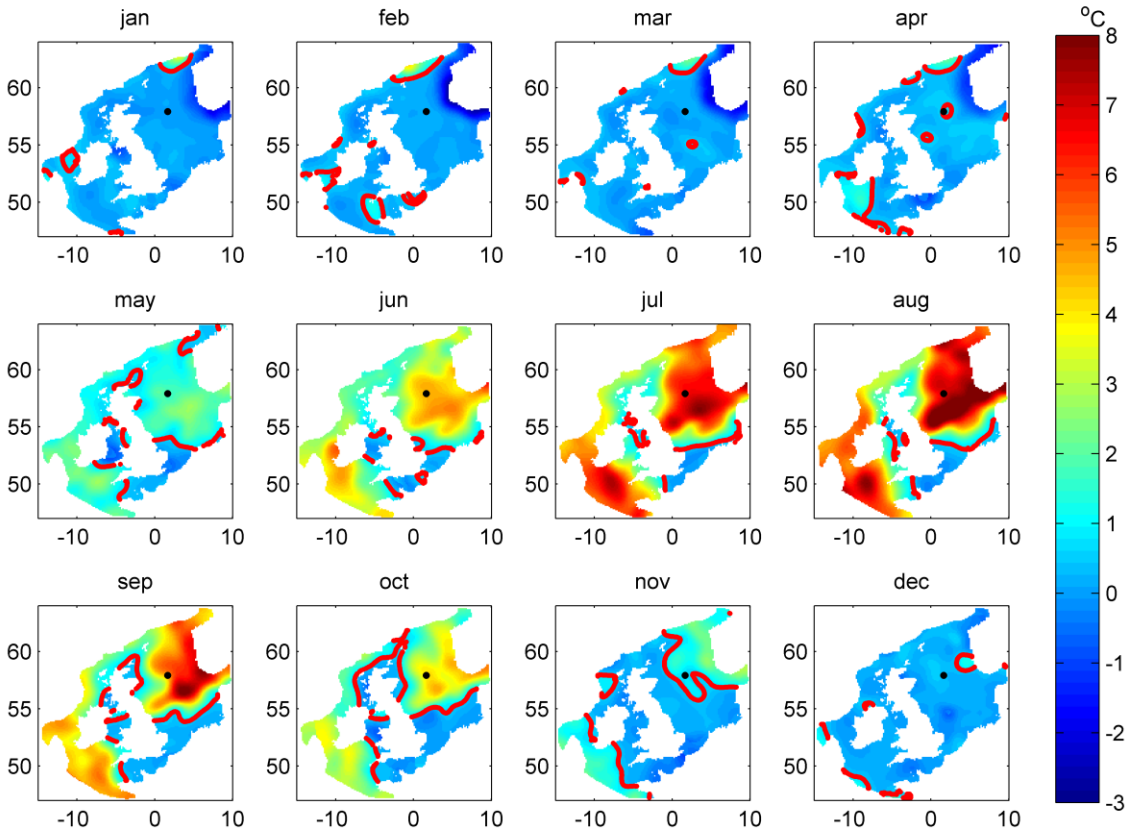

Figure 10: Location of the tidal mixing fronts on the European shelf (red lines) derived with the Berx and hughes (2009) monthly climatology, using the location at which surface to bottom temperature difference equals +0.5°C (Holt and Umlauf, 2008). The map in the back indicates the temperature difference ranging from -3°C (blue) to +8°C (red). The black dot & triangle indicate the locations of the site 22/4b and the PROVESS site in the northern North Sea.

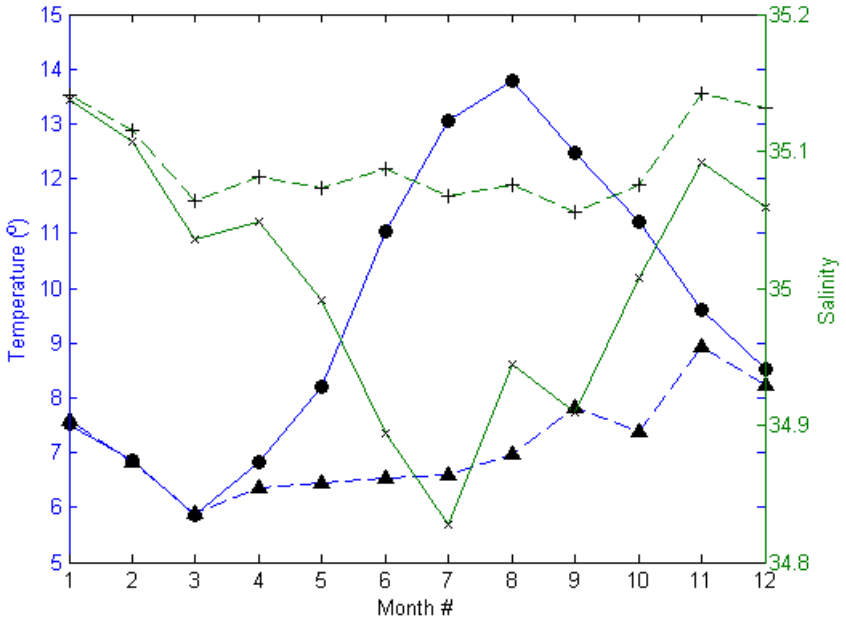

Figure 11: Seasonal variation of the Sea Surface Temperature (bullet symbols), near bed temperature (triangle symbols), sea surface salinity (cross symbols) and near bottom salinity (plus symbols) for site 22/4b from the Berx and Hughes (2009) climatology. Drawn lines mark sea surface values and dashed lines near bottom values.

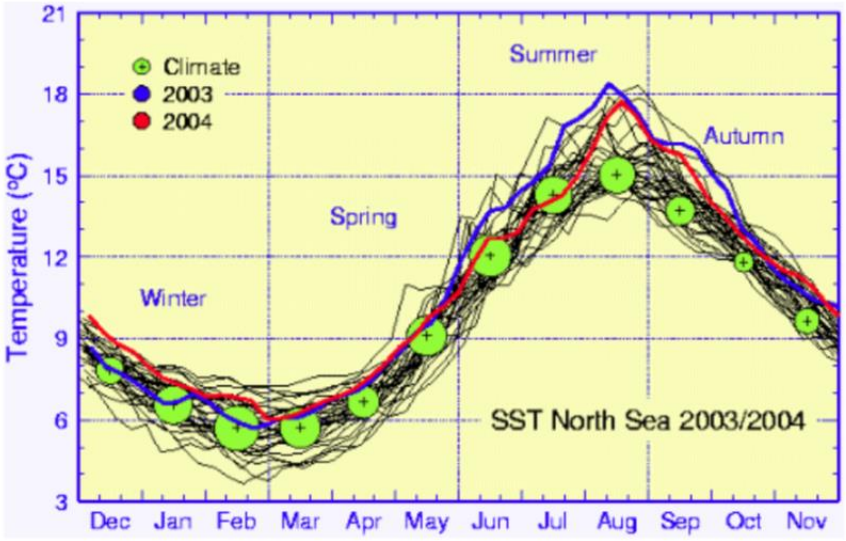

Figure 12: North Sea area averaged SST annual cycle (°C), monthly means based on operational weekly North Sea SST maps. Climatology 1971-1993 is indicated with green dots (the size of the dots is a measure for the standard deviation); blue line indicates 2003, red line indicates 2004; black lines shows individual years, reprinted from Figure 35 on page 28 from ICES (2005).

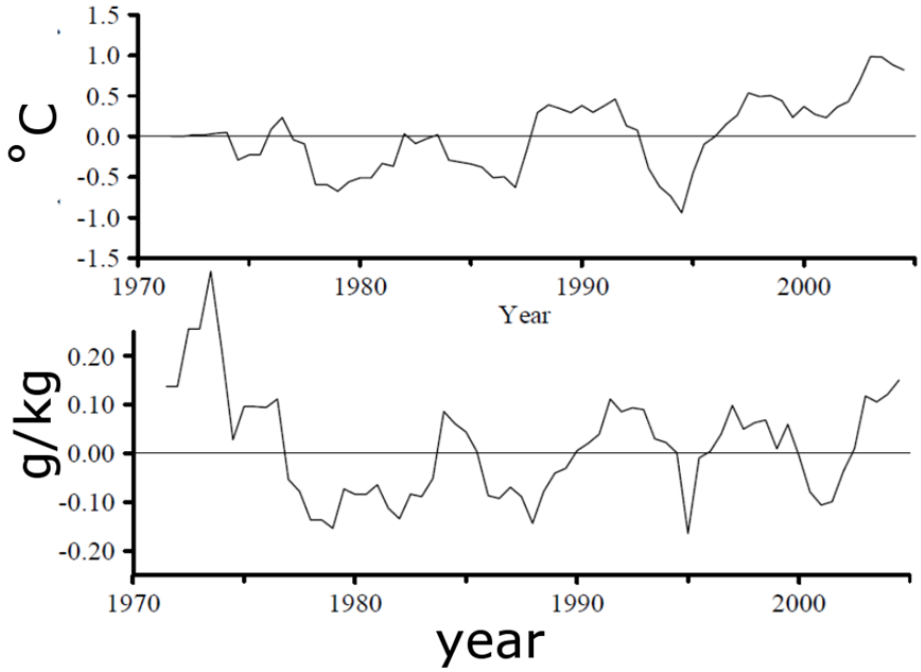

Figure 13: Temperature (°C, top) and Salinity (g/kg, bottom) anomalies in the Fair Isle Current (FIC) entering the North Sea from the North Atlantic reprinted from Figure 36 on page 28 of ICES (2005).

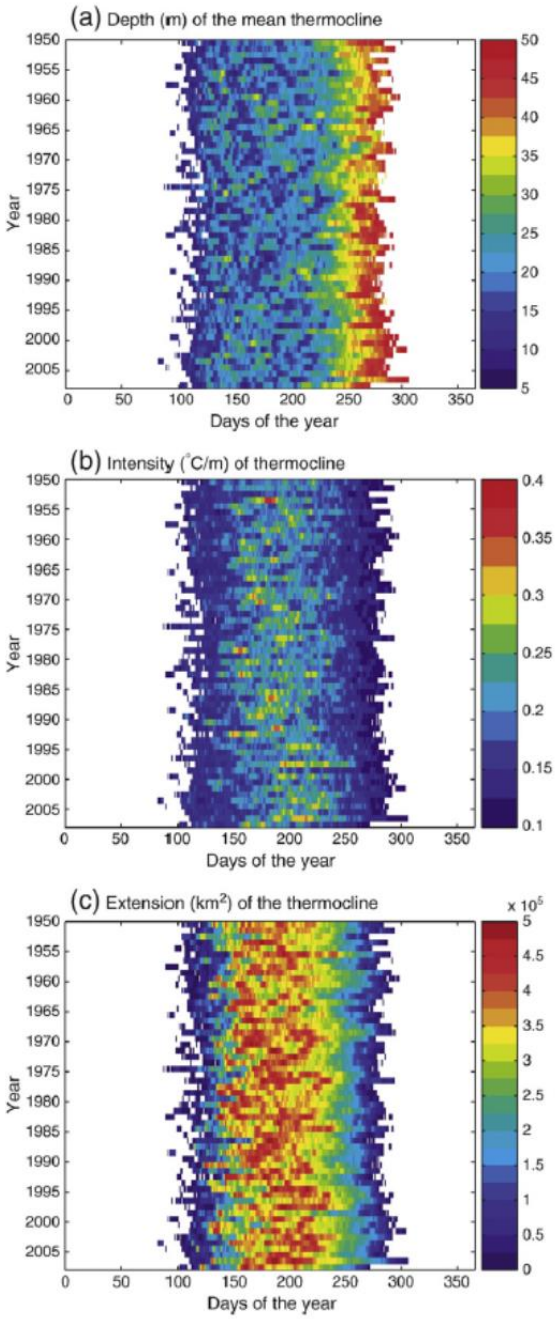

Figure 14: Development of thermocline structure 1950-2007. (a) Depth in m; (b) intensity in $^{o}Cm^{-1}$ and (c) extension in km^2; on the x-axis the days of the year and on the y-axis the years from 1950 to 2007. Reproduced from Figure 8 on page 41 of Meyer et al. (2011).

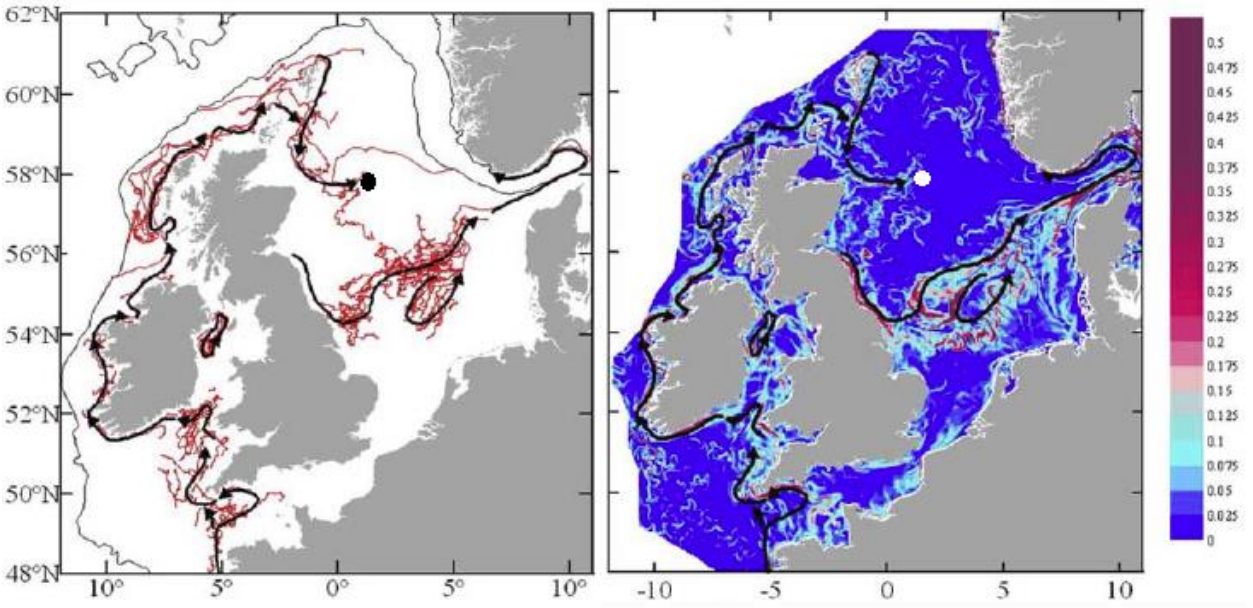

Figure 15: Overview of the shallow thermohaline circulation on the northwest European shelf. (left) Trajectories (red) of 154 satellite tracked drifters. Frontal jets are indicated by black arrows. (right) Frontal jets superimposed on contours of the gradient of bottom horizontal temperature (15 August 2001) derived from a three-dimensional hydrodynamic model (Units – $^{o}C\ km^{-1}$). The black and white dots mark the approximate location of the site 22/4b. This is figure is slightly modified from Figure 2 of (Hill et al., 2008).

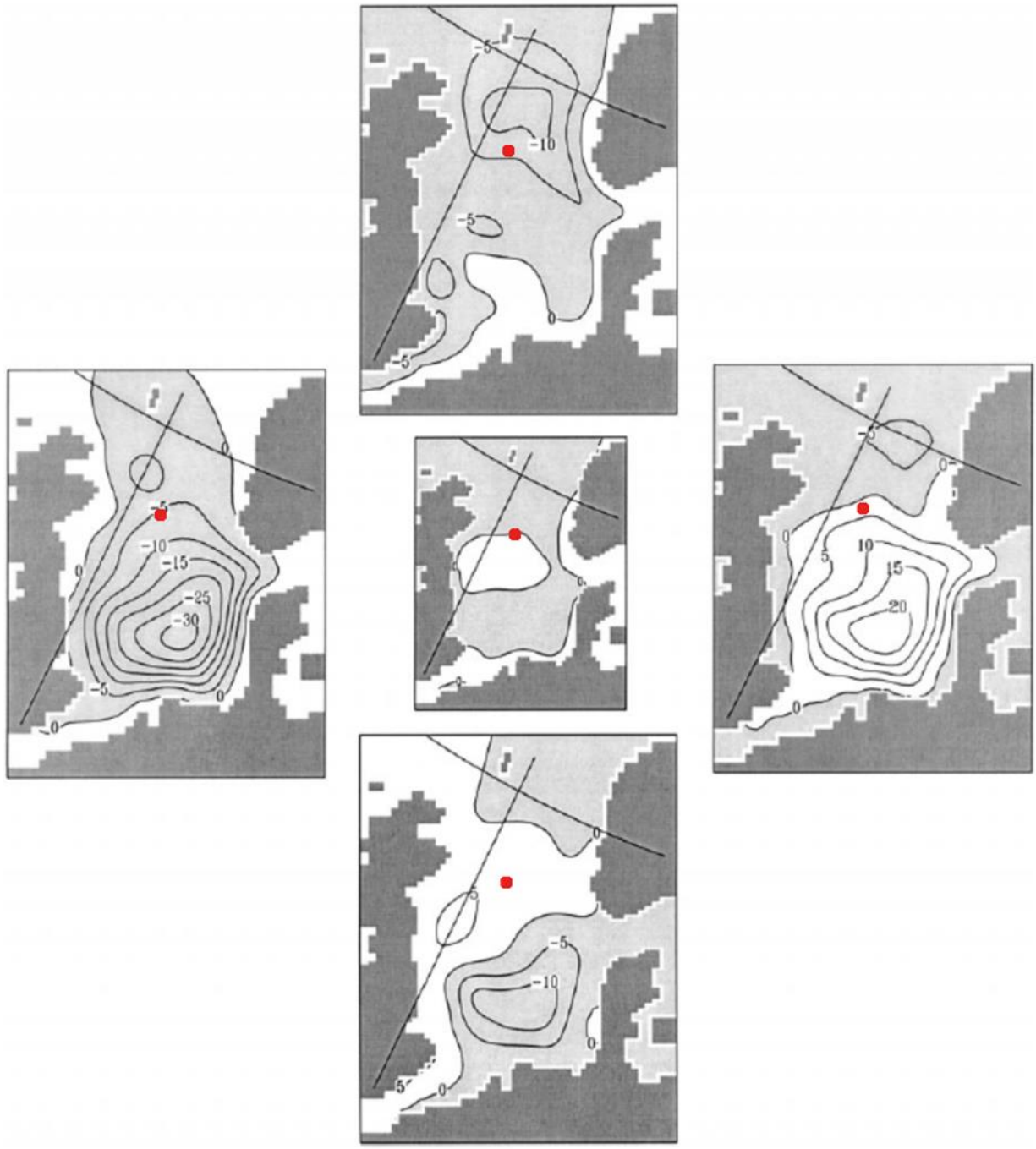

Figure 16: Composites of the first two Extended Orthogonal Functions (EOFs) of streamfunctions for the 5 most dominant circulation patterns of the North Sea circulation. Negative values are shaded and indicate counterclockwise circulation. Units: 10^3 m^2s^{-1}. The red dot marks the approximate location of site 22/4b. For the corresponding mean wind directions and air pressure gradients, see figure 14. This figure is reprinted from Figure 6 on page 3046 of Kauker and von Storch (2000).

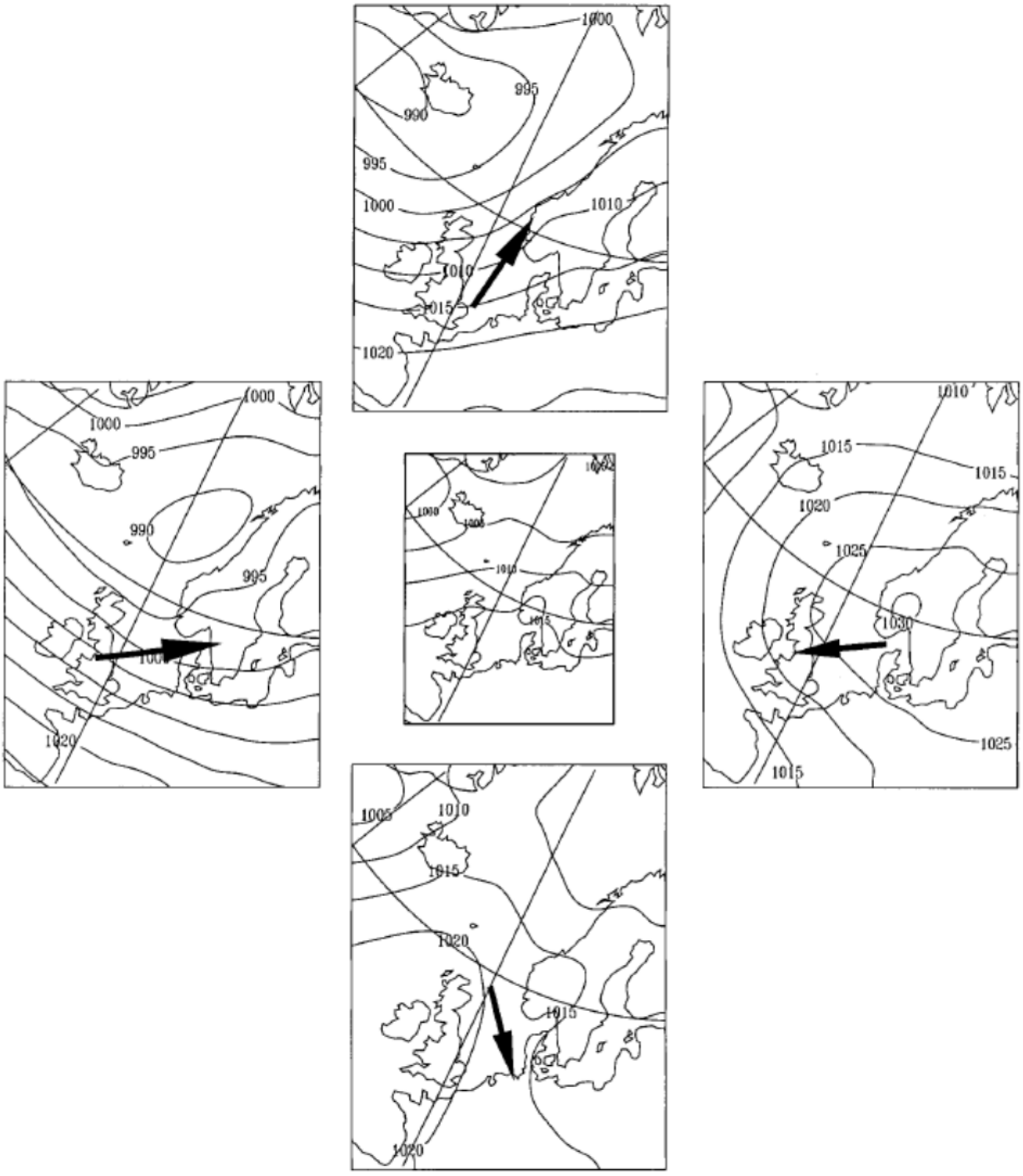

Figure 17: Composites of the pressure distributions and associated dominant wind direction for the 5 dominant circulation patterns shown in Figure 16. Units: hPa. The main direction of the wind stress in analyzed by composites of the wind stress and sketched by the arrow. This figure is reprinted from Figure 7 on page 3047 of Kauker and von Storch (2000).

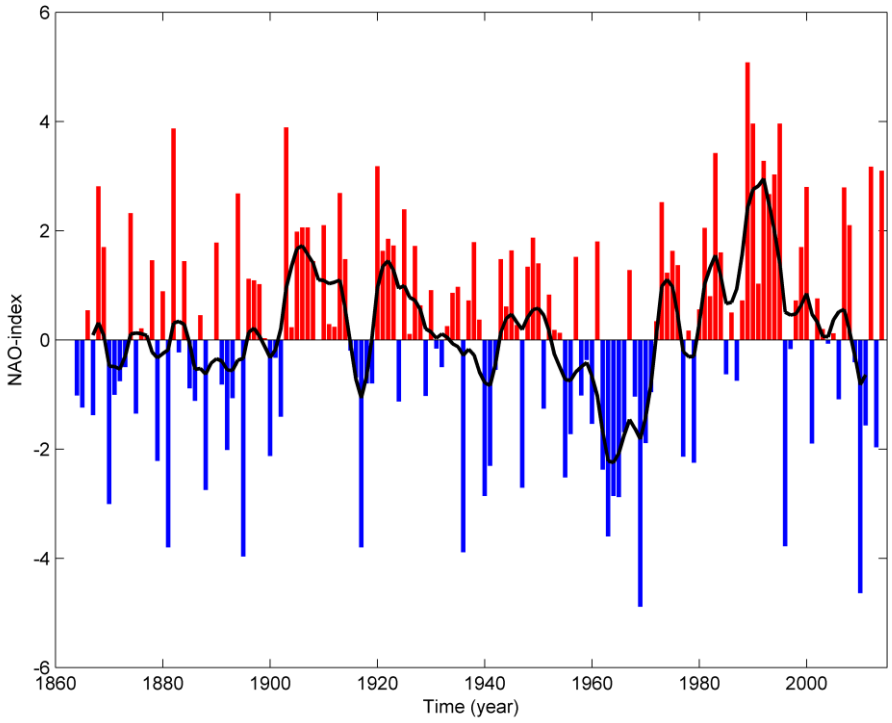

Figure 18: The winter (December to March) NAO index is defined as the normalized pressure difference between Lisbon (Portugal) and Reykjavik (Iceland). The black line shows a five year moving average. Constructed with station-based December January February March (DJFM) North Atlantic Oscillation Index data obtained from http://climatedataguide.ucar.edu/guidance/hurrell-north-atlantic-oscillation-nao-index-station-based.

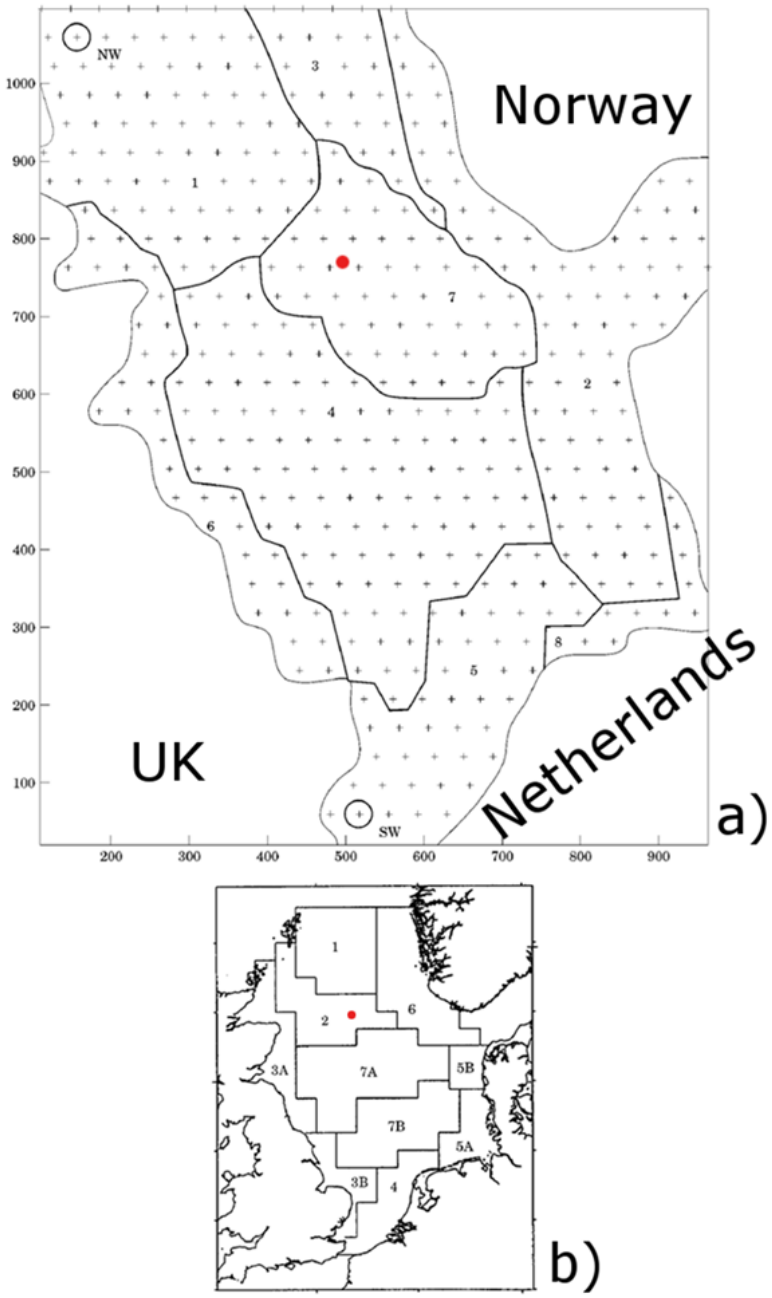

Figure 19: Subdivision of the North Sea in areas as in Becker and Pauly (1996). Top panel: Based on SST patterns; position of 10 selected representative points is indicated by the numbers. Lower panel: Based on hydrographic and biological information (ICES boxes). The red dots mark the approximate location of site 22/4b; reprinted from Figure 4 on page 891 of Becker and Pauly (1996).

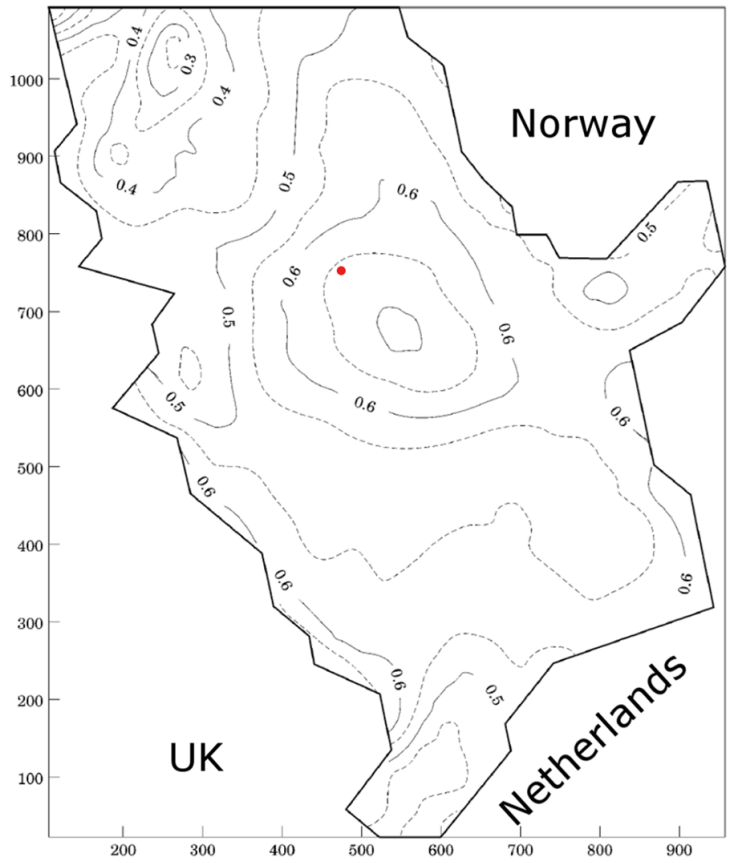

Figure 20: Correlation between NAO index and standardized annual SST anomalies, 1969-1993. The red dot marks the approximate location of site 22/4b; reprinted from Figure 8 on page 895 of Becker and Pauly (1996).

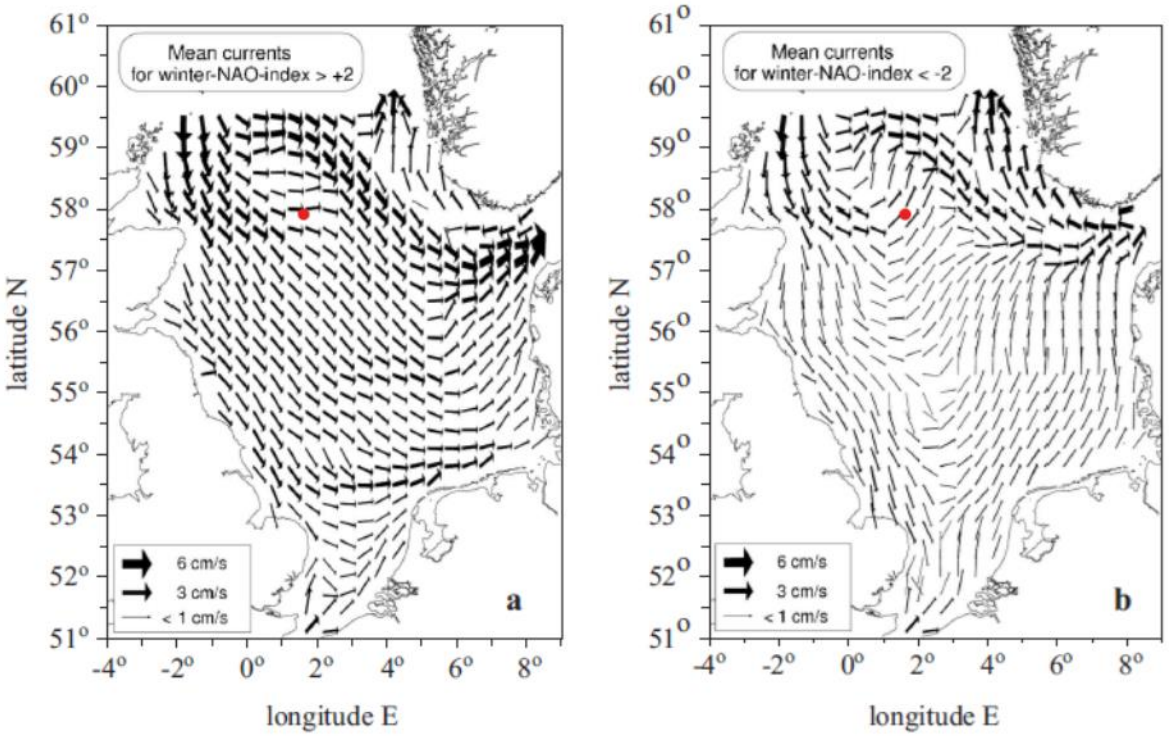

Figure 21: Circulation of the North Sea for different values of the winter NAO index. (a) index > 2. (b) index <-2. The direction of the arrows points in the direction of the flow. The thickness of the arrow indicates the strength of the current. The red dot marks the approximate location of site 22/4b, slightly modified from Figure 7 on page 670 of Sündermann and Pohlmann (2011).

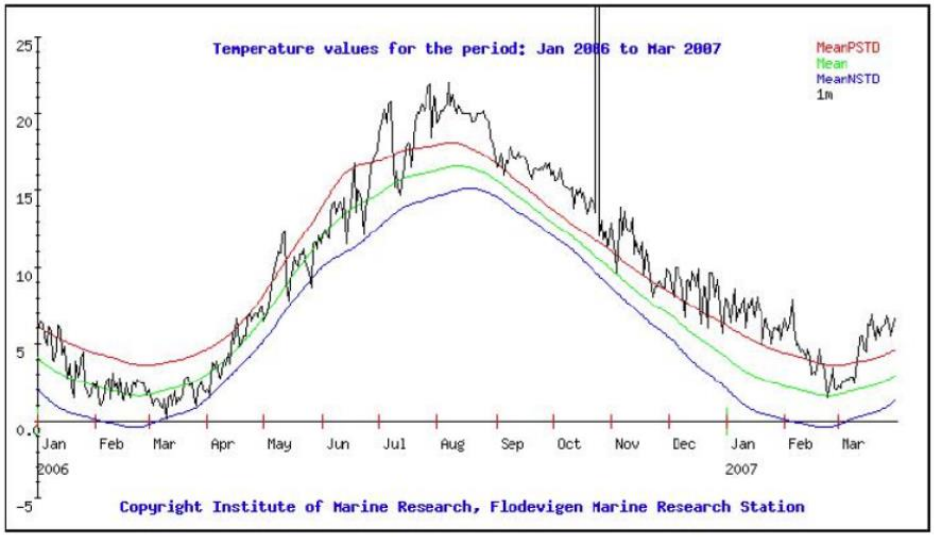

Figure 22: Daily SST recordings at Arendal on the Norwegian Skaggerak coast from January 2005 to December 2006 (black). Also shown is the long-term average temperature (green) +/- 1 SD (standard deviation, blue and red). Units are in °C. The data is from the Norwegian Institute of Marine Research (IMR) and the figure is reprinted from Figure 15 on page 22 of ICES 2007b (2007).

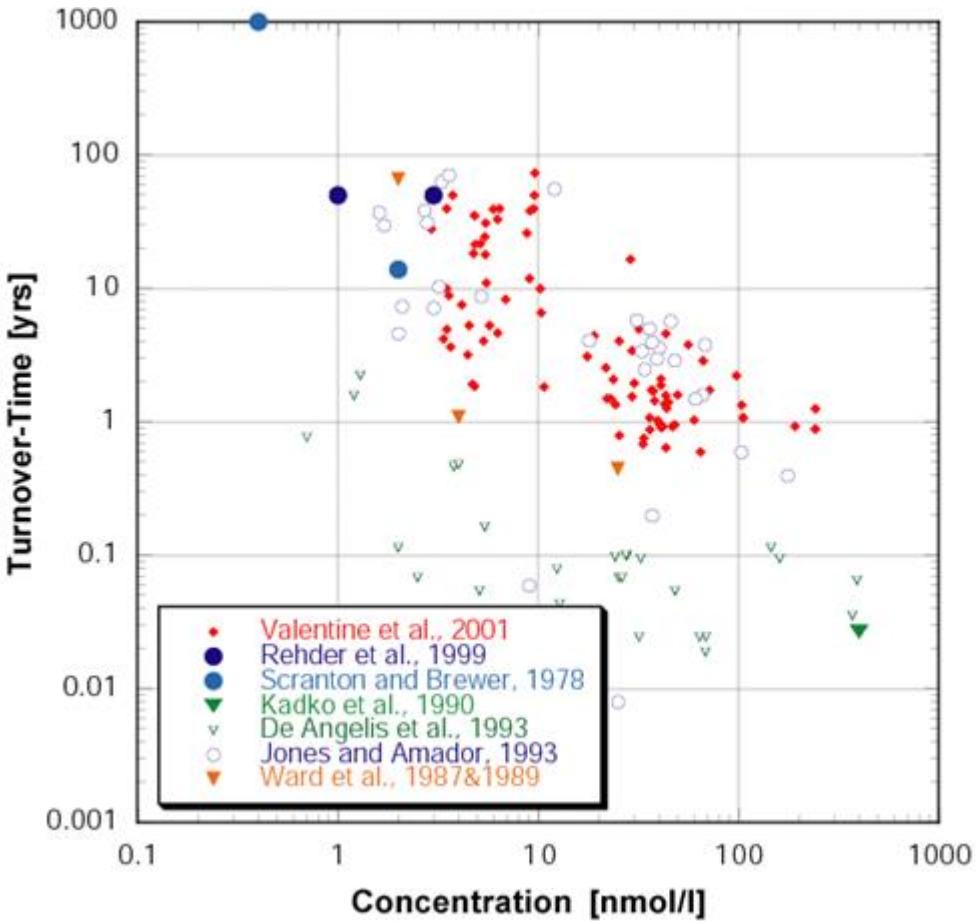

Figure 23: Compilation of reported methane turnover time (1/k) in years versus ambient methane concentration. Note logarithmical scale. Data reported in Ward et al. (1987, 1989), Jones and Amador (1993), Kadko et al. (1990) and De Angelis et al. (1993) were determined using either ^{14}C or ^{3}H labeling techniques, while the studies by Valentine et al. (2001), Rehder et al. (1999) and Scranton and Brewer (1987) were determined using tracer/tracer relations. The studies by Kadko et al. (1990) and De Angelis et al. (1993) are from hydrothermal systems.

Tables

Table 1: Flushing time (days) for ICES box 2.

Study	Minimum	Maximum	Mean
ICES, 1983			109
Backhaus, 1984	9	39	
Prandle, 1984			156
Skogen et al., 1995			50
Luff and Pohlmann, 1995			46
Lenhart and Pohlmann, 1997	14	49	28
Siegismund, 2001			42